Binary inspiral, gravitational radiation, and cosmology

Lee Samuel Finn
Department of Physics and Astronomy,
Northwestern University, Evanston, Illinois 60208-2900
(5 July 1995)

Abstract

Observations of binary inspiral in a single interferometric gravitational wave detector can be cataloged according to signal-to-noise ratio ρ and chirp mass $\mathcal{M}$. The distribution of events in a catalog composed of observations with ρ greater than a threshold ρ_0 depends on the Hubble expansion, deceleration parameter, and cosmological constant, as well as the distribution of component masses in binary systems and evolutionary effects. In this paper I find general expressions, valid in any homogeneous and isotropic cosmological model, for the distribution with ρ and $\mathcal{M}$ of cataloged events; I also evaluate these distributions explicitly for relevant matter-dominated Friedmann-Robertson-Walker models and simple models of the neutron star mass distribution. In matter dominated Friedmann-Robertson-Walker cosmological models advanced LIGO detectors will observe binary neutron star inspiral events with $\rho > 8$ from distances not exceeding approximately 2 Gpc, corresponding to redshifts of 0.48 (0.26) for $h = 0.8$ (0.5), at an estimated rate of 1 per week. As the binary system mass increases so does the distance it can be seen, up to a limit: in a matter dominated Einstein-deSitter cosmological model with $h = 0.8$ (0.5) that limit is approximately $z = 2.7$ (1.7) for binaries consisting of two $10\,\mathrm{M}_\odot$ black holes. Cosmological tests based on catalogs of the kind discussed here depend on the distribution of cataloged events with ρ and $\mathcal{M}$. The distributions found here will play a pivotal role in testing cosmological models against our own universe and in constructing templates for the detection of cosmological inspiraling binary neutron stars and black holes.

PACS numbers: 04.80.Nn, 04.30.Db 97.80.-d, 98.80.Es,

I. INTRODUCTION

A. Overview

The most promising anticipated source for the United States Laser Interferometer Gravitational-wave Observatory (LIGO) [1], or its French/Italian counterpart VIRGO [2], is the radiation emitted during the final moments of inspiral before the coalescence of a neutron star - neutron star (ns-ns) binary system [3]. The instruments operating in both the LIGO and VIRGO facilities will evolve over time, eventually becoming sensitive to neutron star binary inspirals at distances approaching 2 Gpc [4].

Binary inspiral observations in the LIGO or VIRGO detectors will be characterized by their signal strength and "chirp mass" (a combination of the binary's component masses and cosmological redshift). The distribution of observed inspirals with signal strength and chirp mass depends on cosmological parameters that describe our universe (Hubble constant, deceleration parameter, density parameter), the distribution of neutron star masses in binary systems, the overall density of coalescing binaries, and the properties of the detector. In this paper I explore the binary inspiral event distribution (with signal strength and chirp mass) in the LIGO and VIRGO detectors for different cosmological models.

In addition to their value as quantitative expectations of what LIGO and VIRGO can expect to observe, these *a priori* distributions will play a pivotal role both in the construction of templates for detecting binary inspirals and in the interpretation of the observations. The distributions presented here, evaluated for our preconceived notion of the binary inspiral rate and cosmological parameters, are the *prior probabilities* required to form the likelihood function from the observed detector output [4]. Additionally, the observed inspirals will be a sample drawn from a particular cosmological model characterized by H_0, q_0, Ω_0, neutron star mass distribution, and evolution characteristic of our own universe. By comparing the observed distributions to the ones described here we can measure those properties of our own universe[1]

These cosmological tests are analogous to the number-count tests of classical cosmology, which, in their simplest form, involve observing the distribution of a source population as a function of apparent luminosity or redshift. The first suggestion that binary inspiral number counts be used to measure interesting cosmological parameters was made by Finn and Chernoff [4,5] (although they did not use the language usually associated with this technique of classical astronomy). Using Monte Carlo simulations they demonstrated that the distribution of inspiral events with signal strength and chirp mass could be used to measure the Hubble constant. In this work I provide a more general, explicit, and complete exposition of the properties of binary inspiral observation catalogs.

---

[1]A detailed study of how accurately those measurements can be made as a function of the number of inspiral observations is underway and will be published separately; here I focus on describing the properties of a catalog of observations defined by a data cut on the signal-to-noise ratio and how those properties can be used to measure cosmological parameters.

The cosmological implications of gravitational wave observations of binary inspiral were first recognized by Schutz [6]. He pointed out that each inspiraling binary is a standard candle in the sense that, if observed in three independent interferometers, its luminosity distance can be determined from the observed detector response. If an observed inspiral is associated with one of the several galaxy clusters that reside in its positional error box (whose determination also requires three interferometers), and if the redshifts of those clusters are determined optically, then observation of several inspiraling binaries would lead to a statistical determination of the Hubble constant that is independent of the cosmic distance ladder and the uncertainties that lurk therein.

Marković [7] proposed a variation on the general theme introduced by Schutz: he observed that known neutron star masses were all close to $1.4\,M_\odot$ and that, in any event, there is a *maximum* neutron star mass. The observed chirp mass is a function of the mass of the binary's two components and its redshift. Assuming that the mass distribution in neutron star binaries does not evolve significantly over the range of binary inspiral observations, examination of the chirp mass distribution in binary systems at fixed luminosity distance would reveal the corresponding redshift. Thus, gravitational radiation observations alone might suffice to determine the Hubble constant.

Unfortunately, detailed calculations show that, even for the most advanced LIGO and VIRGO detectors that have been discussed, the fractional uncertainty in the measured luminosity distance will be of order unity for events seen more frequently than thrice per year (*i.e.,* for events at distances greater than approximately 100 Mpc) [8,9], and the angular position error boxes for these events are likewise large (on order 10 deg^2 [10]). Consequently, cosmological tests that rely on accurate and precise measurements of the distance and position of inspiraling binaries using LIGO and VIRGO are not promising.

In contrast, the cosmological tests discussed here and in [5] require only gravitational wave observation in a single interferometer. Furthermore, advanced LIGO detectors can expect to observe approximately 50 ns-ns binary inspiral events per year, from distances up to 2 Gpc, whose signal strength can be measured to better than 10% and whose chirp mass can be measured to better than 0.1% [4,9]. The rate, depth, accuracy and precision of these single interferometer observations suggest that cosmological tests based on the distribution of observed events with signal strength and chirp mass have great promise.

B. Outline

In this paper I calculate the expected properties of a catalog of binary inspiral observations made by a single interferometric gravitational wave detector. A catalog is presumed to contain a record of all binaries that coalesced during the observation period and whose inspiral signal-to-noise ratio ρ was greater than the catalog limit ρ_0. The catalog properties depend on the coalescence rate density and the binary system component mass distribution, both of which may vary with redshift. Notation for these and a discussion of the observations that bear on them is the topic of section II.

In section III I discuss the signal-to-noise ratio ρ as a measure of signal strength. The signal-to-noise ratio of a particular inspiraling binary depends on the binary's intrinsic properties, its distance from and orientation with respect to the detector, and the detector's

intrinsic properties. The way in which ρ depends on the signal and detector properties suggests a useful measure of the detector bandwidth, which I discuss here as well. Finally, section III concludes by specializing the discussion to the specific properties of the proposed LIGO and VIRGO gravitational radiation detectors.

The important properties of a binary inspiral observation catalog are the distribution of cataloged events with ρ and the binary system "chirp mass" $\mathcal{M}$. These distributions depend on the cosmological model, which includes the evolution with redshift of the neutron star mass distribution and the coalescing binary number density. In section IV I give general expression for these distributions and discuss how they may be used together with actual observations to test cosmological models. Also in this section I give expressions for the *catalog depth* (the maximum redshift of a binary system that can have ρ greater than ρ_0) and the total rate that proposed interferometers can expect to observe inspiraling binaries with ρ greater than ρ_0. All of these general expressions are evaluated explicitly for relevant matter-dominated Friedmann-Robertson-Walker cosmological models and a simple model of the neutron star mass distribution. Finally, I summarize my conclusions in section V.

II. COALESCENCE RATE DENSITY

A. Introduction

The signal-to-noise ratio ρ of a binary inspiral in a LIGO-like interferometer depends on the relationship between the binary and the detector (*i.e.,* orientation, distance and redshift) and also on certain intrinsic properties of the system (*i.e.,* component masses and spins). Of these intrinsic properties, the *intrinsic chirp mass,*

$$\mathcal{M}_0 \equiv \mu^{3/5} M^{2/5} \tag{2.1}$$

where μ and M are the binary's reduced and total mass, plays the most important role: all the other intrinsic properties offer only small corrections to ρ.

Gravitational-wave detectors like LIGO or VIRGO do not measure $\mathcal{M}_0$; instead, they measure

$$\mathcal{M} \equiv \mathcal{M}_0(1+z), \tag{2.2}$$

where z is the system's redshift with respect to the detector. To distinguish between $\mathcal{M}$, which involves the system's redshift, and $\mathcal{M}_0$, which depends only on the binary's intrinsic properties, I refer to the former as the *observed* chirp mass, or simply the chirp mass, and the latter as the *intrinsic* chirp mass.

In order to describe the binaries included in a signal-to-noise limited catalog we must first describe the coalescing binary distribution in space and in $\mathcal{M}_0$. The notation I use to describe this distribution is defined in section II B, while in section II C I discuss what is known about the distribution from present-day observations.

B. Definitions and notation

Assume that coalescing binaries are distributed homogeneously and isotropically with the cosmological fluid and define the binary coalescence *local specific rate density* $\mathcal{N}$ by

$$\mathcal{N} \equiv \frac{d^3N}{dt\, dV\, d\mathcal{M}_0}, \tag{2.3}$$

where dV is a *co-moving* cosmological fluid volume element and dt is a proper time interval measured in the fluid rest frame. The total co-moving rate density on the surface of homogeneity at redshift z is thus

$$\dot{n}(z) = \int \mathcal{N}(\mathcal{M}_0, z)\, d\mathcal{M}_0. \tag{2.4}$$

Define the ratio of the total co-moving rate density at a redshift z $[\dot{n}(z)]$ to that at the present epoch $[\dot{n}_0 = \dot{n}(z=0)]$ by $\mathcal{E}$:

$$\dot{n}(z) = \mathcal{E}(z)\dot{n}_0. \tag{2.5}$$

The distribution of coalescing binaries with intrinsic chirp mass $\mathcal{M}_0$ on the surface at redshift z is

$$\mathcal{P}(\mathcal{M}_0|z) = \frac{\mathcal{N}(\mathcal{M}_0, z)}{\dot{n}(z)}, \tag{2.6}$$

where, by construction,

$$1 = \int d\mathcal{M}_0\, \mathcal{P}(\mathcal{M}_0|z). \tag{2.7}$$

The homogeneous and isotropic local specific rate density can thus be written

$$\mathcal{N}(\mathcal{M}_0, z) = \dot{n}_0 \mathcal{E}(z) \mathcal{P}(\mathcal{M}_0|z). \tag{2.8}$$

Since we have defined $\mathcal{N}$ and $\dot{n}$ in terms of the co-moving volume element and intrinsic chirp mass, in the absence of evolution $\mathcal{E}$ is unity and $\mathcal{P}$ is independent of z. Additionally, for infinitesimal $d\mathcal{M}_0$, $\mathcal{P}(\mathcal{M}_0|z)d\mathcal{M}_0$ can be interpreted as the probability that a randomly chosen binary on the surface at redshift z has intrinsic chirp mass in the range $\mathcal{M}_0$ to $\mathcal{M}_0 + d\mathcal{M}_0$.

C. Observational constraints on $\mathcal{N}$

1. Rate density at the current epoch: $\dot{n}_0$

Cosmological tests that depend on the observed *distribution* of inspirals with ρ and/or $\mathcal{M}$ do not depend on $\dot{n}_0$. Nevertheless, it is necessary to know $\dot{n}_0$ in order to estimate how

long it will take to accumulate a catalog of observations large enough that such tests will give meaningful results.

The best current estimate of the ns-ns binary coalescence rate density at the current epoch is $1.1 \times 10^{-8} h\,\mathrm{Mpc}^{-3}\ \mathrm{yr}^{-1}$, where h is the Hubble constant measured in units of $100\,\mathrm{Km\,s}^{-1}\,\mathrm{Mpc}^{-1}$ [11,12]. This estimates relies on the 3 observed binary pulsar systems that will coalesce in less than a Hubble time (PSRs 1913+16, 1534+12, and 2127+11C [13–15]). Since the number of observed systems is small the actual rate is quite uncertain: Phinney [12] has estimated that, while unlikely, a rate two orders of magnitude higher or lower could be reconciled with current observations.

Black hole - black hole (bh-bh) and bh-ns binaries are believed to form at rates comparable to ns-ns binaries; however, the masses of these systems and the fraction that merge in less than a Hubble time are entirely uncertain [11,12].

2. Intrinsic chirp mass distribution and evolution: $\mathcal{P}$ and $\mathcal{E}$

The intrinsic chirp mass distribution $\mathcal{P}(\mathcal{M}_0|z)$ depends on the binary system component mass distribution on the slice of homogeneity at redshift z. Denote a binary's component masses as m_1 and m_2 and write their joint probability density on a surface of redshift z as $P(m_1, m_2|z)$. The intrinsic chirp mass distribution $\mathcal{P}(\mathcal{M}_0|z)$ on that slice is then

$$\mathcal{P}(\mathcal{M}_0|z) = \iint dm_1\, dm_2\, P(m_1, m_2|z) \times \delta\big(\mu^{3/5} M^{2/5} - \mathcal{M}_0\big)\,. \tag{2.9}$$

The determination of $\mathcal{P}(\mathcal{M}_0|z)$ thus reduces to finding $P(m_1, m_2|z)$.

Both theoretical and observational evidence suggest that the neutron star mass distribution is narrow [16–18]. A simple model of the mass distribution has the component masses in a binary uncorrelated and uniformly distributed between upper and lower bounds m_u and m_l; then

$$\begin{aligned} P(m_1, m_2|m_l, m_u) &= P(m_1|m_l, m_u) P(m_2|m_l, m_u) \\ &= (m_u - m_l)^{-2} \end{aligned} \tag{2.10}$$

and

$$P(\mathcal{M}_0|m_l, m_u) = \int_{m_l}^{m_u}\int_{m_l}^{m_u} dm_1\, dm_2 \frac{\delta\left[\left(\frac{m_2^3 m_1^3}{m_1+m_2}\right)^{1/5} - \mathcal{M}_0\right]}{(m_u - m_l)^2}. \tag{2.11}$$

where m_l and m_u may depend on z. The probability density $P(\mathcal{M}_0|m_l, m_u)$ is maximized when $\mathcal{M}_0 = (m_l m_u)^{3/5}/(m_l + m_u)^{1/5}$.

The limited observations of the neutron star mass distribution in binary pulsar systems provide independent 95% confidence intervals for m_l and m_u [17]:

$$\begin{aligned} 1.01 \;&<\; m_l/\mathrm{M}_\odot \;<\; 1.34 \\ 1.43 \;&<\; m_u/\mathrm{M}_\odot \;<\; 1.64. \end{aligned} \tag{2.12}$$

The most likely values of m_l and m_u are

$$\begin{aligned} m_l \;&=\; 1.29\,\mathrm{M}_\odot, \\ m_u \;&=\; 1.45\,\mathrm{M}_\odot. \end{aligned} \tag{2.13}$$

Over this narrow range $P(\mathcal{M}_0|m_l, m_u)$ is, to an excellent approximation, piecewise linear:

$$P(\mathcal{M}_0|m_l, m_u) \simeq \frac{2}{m_> - m_<} \begin{cases} \frac{\mathcal{M}_0 - m_<}{m_0 - m_<} & \text{if } m_0 > \mathcal{M}_0 > m_<, \\ \frac{m_> - \mathcal{M}_0}{m_> - m_0} & \text{if } m_> > \mathcal{M}_0 > m_0, \\ 0 & \text{otherwise} \end{cases} \tag{2.14}$$

where

$$m_< \equiv m_l/2^{1/5}, \tag{2.15a}$$

$$m_0 \equiv \frac{(m_l m_u)^{3/5}}{(m_l + m_u)^{1/5}} \tag{2.15b}$$

$$m_> \equiv m_u/2^{1/5}. \tag{2.15c}$$

At present we can observe only nearby binary pulsar systems; consequently, there are no observations that bear directly on the variation of $\mathcal{E}$ or $\mathcal{P}$ with z. Theoretical studies suggest that the initial mass of neutron stars formed by stellar core collapse do not vary significantly with the progenitor mass or composition [16]. After formation the mass may evolve owing to accretion from a companion; however, in any event it is not likely that either $\mathcal{P}$ or $\mathcal{E}$ vary with z more rapidly than do galaxies. In section IV I provide general expressions for and detailed examples of the expected distribution of events in a catalog of binary inspiral events; for the detailed examples I neglect evolution in $\mathcal{E}$ and $\mathcal{P}$ entirely. As shown in section IV D, advanced LIGO and VIRGO detectors will observe ns-ns binaries from redshifts not expected to exceed $z \simeq 0.5$ and with the preponderance of events arising from $z \simeq 0.1$; consequently, neglect of evolution is not an unreasonable approximation.

III. THE SIGNAL-TO-NOISE RATIO

A. Outline

The signal-to-noise ratio measures the signal amplitude in terms of a detector's noise properties. In subsection III B I define the signal-to-noise ratio ρ and discuss the subtle issue of how ρ is estimated, but not determined, by observation. The functional form of ρ depends on the detector response to binary inspiral radiation, which I describe in subsection III C. In subsection III D I give the binary inspiral signal-to-noise ratio in terms of the same parameters that characterize the detector response. The form of ρ suggests a natural

definition of a detector's effective bandwidth for binary inspiral observations; I discuss this bandwidth function in subsection III D as well.

The relative orientation of the detector and binary is described by a function of four angles. While these angles cannot be measured by observations in a single interferometer, important properties of the angular orientation function can be calculated independently of the particulars of the binary or the detector. These properties play an important role in determining the binary inspiral catalog properties and interpreting individual observations. I discuss the angular orientation function in subsection III E.

Finally, in subsection III F I specialize the discussion of the signal-to-noise to the proposed LIGO and VIRGO gravitational radiation detectors.

B. The signal-to-noise ratio: general comments

Let $s(t)$ be the detector response to a gravitational radiation signal from any source. If the detector noise is Gaussian with one-sided power spectral density $S_n(f)$ then the signal-to-noise ratio ρ^2 is *defined* to be

$$\rho^2 = 2\int_{-\infty}^{\infty} \frac{\widetilde{s}(f)\widetilde{s}^*(f)}{S_n(|f|)} df, \tag{3.1}$$

where $\widetilde{s}$ is the Fourier transform of the detector response,

$$\widetilde{s}(f) \equiv \int_{-\infty}^{\infty} df\, e^{2\pi i f t} s(t), \tag{3.2}$$

and $\widetilde{s}^*$ is its complex conjugate [19].

An observation of a gravitational wave signal in a noisy detector entails a measurement of the signal properties in the presence of a particular instance of the detector noise. Analysis of the detector output results in an *estimate* of ρ as well as other parameters that describe $s(t)$. *Throughout this work I use ρ to mean the actual signal-to-noise ratio, as defined by equation 3.1, and not the estimate that arises in an observation.*

In section IV I find the distribution of sources with ρ and $\mathcal{M}$ in different cosmological models. By comparing these distributions with the observed one we can determine the model that best describes our own universe. In making that comparison it is critical to distinguish between ρ and $\mathcal{M}$ (as *defined* by equations 3.1 and 2.2) and the *estimates* of ρ and $\mathcal{M}$ that results from observations made in a detector.

The estimate that results from an observation is a probability distribution P for the parameters that describe the signal — in the case of binary inspiral in a single interferometer, these include ρ and the chirp mass $\mathcal{M}$ (see sec. III C below). The probability distribution associated with an observation is generally not reported; instead, what is reported most often is a set of *estimators* that characterize the distribution and its moments. Among the most popular is the the maximum likelihood estimator, which is the set of parameter values that maximize P.

Estimators are summaries of the distribution P and their utility depends on how accurately they are able to represent it. When P is very sharply peaked (*i.e.,* there is little

uncertainty in the measurement) then it may be approximated by a δ-function and summarized accurately by the maximum likelihood estimator. When P is sharply peaked but with a not insignificant width, then it may be approximated near its peak by a Gaussian and accurately represented by the maximum likelihood estimators and their covariance. When the distribution is not sharply peaked, however, then the more general uncertainties reflected in the detailed structure of P play an essential role in the observation's interpretation and no summary of P is especially useful.

That a small set of estimators built from P for a particular observation do not provide a useful summary does not mean that the observation itself is unreliable or uninformative; rather, it means only that greater care must be taken in its interpretation. Finn [20, sec. (c)] gives an example of how the the probability distribution resulting from an observation should be used in the interpretation of neutron star mass observations in binary pulsar systems; a further discussion of this point in the context of cosmological tests using binary inspiral observation catalogs is part of a work in preparation.

C. Detector response to binary inspiral

The detector response $s(t)$ to the gravitational radiation from an inspiraling binary system depends on the distance and relative orientation of the source and the detector, as well as on certain intrinsic properties of the binary. The relative orientation of the source and the detector is described by four angles: two (θ and ϕ) describe the direction to the binary relative to the detector, and two (i and ψ) describe the binary's orientation relative to the line-of-sight between it and the detector.

To describe θ and ϕ, consider a single interferometric gravitational wave detector whose arms form a right angle. Let the arms themselves determine the $\boldsymbol{x}$ and $\boldsymbol{y}$ axes of a right-handed Cartesian coordinate system with the $\boldsymbol{z}$-axis pointing skyward. In this coordinate system the gravitational waves from an inspiraling binary arrive from the direction $\boldsymbol{n}$, which can be defined in terms of the spherical coordinates θ and ϕ in the usual way:

$$\cos\theta \equiv -\boldsymbol{n}\cdot\boldsymbol{z}, \tag{3.3a}$$

$$\tan\phi \equiv \frac{\boldsymbol{n}\cdot\boldsymbol{y}}{\boldsymbol{n}\cdot\boldsymbol{x}}. \tag{3.3b}$$

To describe i and ψ, let $\boldsymbol{J}$ represent the total angular momentum of the binary system. The detector response $s(t)$ depends on the *inclination angle* i between $\boldsymbol{J}$ and $\boldsymbol{n}$,

$$\cos i \equiv -\boldsymbol{J}\cdot\boldsymbol{n}/|\boldsymbol{J}|, \tag{3.3c}$$

and the orientation ψ of the angular momentum about $\boldsymbol{n}$,

$$\cot\psi \equiv \frac{\boldsymbol{J}\cdot\boldsymbol{n}\times\boldsymbol{z}}{\boldsymbol{J}\cdot[\boldsymbol{z}-\boldsymbol{n}(\boldsymbol{z}\cdot\boldsymbol{n})]}. \tag{3.3d}$$

The conventions for the orientation angles θ, ϕ, i, and ψ described here are the same as those used in [3,4] (note, however, that the *description* of the angles in [4] is incorrect).

At Newtonian (*i.e.,* quadrupole formula) order the only intrinsic property of the binary system that affects the waveform is $\mathcal{M}_0$. At this order the detector response (a dimensionless strain) to the binary inspiral signal is

$$s(t) = \begin{cases} \frac{\mathcal{M}}{d_L}\Theta\left(\pi f \mathcal{M}\right)^{2/3}\cos\left[\chi + \Phi(t)\right] & \text{for } t < T', \\ 0 & \text{for } t > T', \end{cases} \tag{3.4a}$$

where χ is a constant phase,

$$\Theta \equiv 2\left[F_+^2\left(1+\cos^2 i\right)^2 + 4F_\times^2\cos^2 i\right]^{1/2}, \tag{3.4b}$$

$$F_+ \equiv \frac{1}{2}\left(1+\cos^2\theta\right)\cos 2\phi\cos 2\psi - \cos\theta\sin 2\phi\sin 2\psi, \tag{3.4c}$$

$$F_\times \equiv \frac{1}{2}\left(1+\cos^2\theta\right)\cos 2\phi\sin 2\psi + \cos\theta\sin 2\phi\cos 2\psi, \tag{3.4d}$$

$$f = \frac{1}{\pi\mathcal{M}}\left[\frac{5}{256}\frac{\mathcal{M}}{T-t}\right]^{3/8}, \tag{3.4e}$$

$$\Phi \equiv 2\pi\int_T^t f(t)dt = -2\left(\frac{T-t}{5\mathcal{M}}\right)^{5/8}, \tag{3.4f}$$

d_L is the source's luminosity distance, T' is the moment when the inspiral waveform terminates (either because the binary components have coalesced or because the orbital evolution is no longer adiabatic), and $T > T'$ would be the moment of coalescence if the two components of the binary system were treated as point masses in the quadrupole approximation (the difference between T and T' is small but not negligible). Note that dependence of the response on the angles θ, ϕ, i, and ψ is contained entirely in the orientation function Θ, which does not depend on any other properties of the binary or the interferometric detector. This important point will be discussed further in subsection III E.

Post-Newtonian corrections do not contribute significantly to the signal-to-noise ratio for solar-mass binary inspiral in the LIGO and VIRGO interferometers. For symmetric binaries (*i.e.,* those with equal or near equal mass components) the first post-Newtonian correction is proportional to M/r, where M is the binary's total mass and r the component separation. Advanced LIGO and VIRGO interferometers are expected to be most sensitive to binary inspiral radiation in the bandwidth 20–200 Hz (see sec. III D 2) and, in this bandwidth, $M/r \lesssim 4\%$ for solar mass binaries. Post-Newtonian effects are more important for more massive binaries, since at fixed quadrupole radiation frequency M/r is greater for greater M:

$$\left(\frac{M}{r}\right) \simeq \left(\pi f M\right)^{1/3} \tag{3.5a}$$

$$\simeq 0.042\left(\frac{f}{200\,\mathrm{Hz}}\frac{M}{2.8\,\mathrm{M}_\odot}\right)^{2/3} \tag{3.5b}$$

$$\simeq 0.16\left(\frac{f}{200\,\mathrm{Hz}}\frac{M}{20\,\mathrm{M}_\odot}\right)^{2/3}. \tag{3.5c}$$

Post-Newtonian effects are more important for binaries with extreme mass ratios: in general, the first post-Newtonian correction is proportional to $(\delta m/M)(M/r)^{1/2}$, where δm is the component mass difference. Finally, spin-orbit coupling in systems whose components have large spin angular momenta can lead to orbital precession and a waveform modulation which can affect ρ significantly [21].

That the quadrupole waveform can be used to *estimate* ρ for an inspiraling binary does not mean it can also be used to *detect* a binary inspiral signal in the detector output. Detection, or estimation of signal parameters from observation, involves the comparison of the detector output with a model of the detector response to the radiation. "Small" differences between the actual and modeled signal evolution, particularly its phase, can have a large effect on the measured value of the signal parameters, including the signal-to-noise ratio estimated from the observations [4,22].

D. Binary inspiral signal-to-noise ratio

The signal-to-noise ratio ρ (eq. 3.1) corresponding to the detector response $s(t)$ (eq. 3.4a) is [4]

$$\rho = 8\Theta \frac{r_0}{d_L} \left(\frac{\mathcal{M}}{1.2\,\mathrm{M}_\odot} \right)^{5/6} \zeta(f_{\max}), \tag{3.6a}$$

where

$$r_0^2 \equiv \frac{5}{192\pi} \left(\frac{3}{20} \right)^{5/3} x_{7/3} \mathrm{M}_\odot^2, \tag{3.6b}$$

$$x_{7/3} \equiv \int_0^\infty \frac{df\ (\pi \mathrm{M}_\odot)^2}{(\pi f \mathrm{M}_\odot)^{7/3}\, S_n(f)}, \tag{3.6c}$$

$$f_{\max} = f(T')/2, \tag{3.6d}$$

$$\zeta(f_{\max}) \equiv \frac{1}{x_{7/3}} \int_0^{2f_{\max}} \frac{df\ (\pi \mathrm{M}_\odot)^2}{(\pi f \mathrm{M}_\odot)^{7/3}\, S_n(f)}. \tag{3.6e}$$

In equation 3.6a Θ, $\mathcal{M}$ and d_L depend on the particular binary system under consideration and r_0 is a characteristic distance that depends only on the detector's noise power spectral density $S_n(f)$. The dimensionless function ζ, which also depends only on the detector's noise spectrum, increases monotonically from 0 to 1. Its argument $f_{\max}$ is the redshifted instantaneous orbital frequency when the inspiral terminates (at $t = T'$) either because the compact components have coalesced or because the orbital evolution is no longer adiabatic and coalescence is imminent.

1. r_0 and ζ

The characteristic distance r_0 and the function ζ describe different aspects of an interferometric detectors sensitivity to binary inspiral gravitational radiation. For a fixed binary,

the larger r_0, the greater ρ; for fixed ρ, the larger r_0, the farther the detector can "see." Decreasing the noise power in any band increases r_0, but (owing to the factor $f^{-7/3}$ in the integrand of the expression for $x_{7/3}$) improvements at low frequency are more effective than those high frequency.

The function ζ reflects the overlap of the signal power with the detector bandwidth. The orbit of an inspiraling compact binary evolves adiabatically owing to gravitational radiation emission until an innermost circular orbit (ICO) is reached at an instantaneous orbital frequency $f_{\rm ICO}$. At the ICO the orbit evolves on a dynamic timescale and the components coalesce quickly. Thus, the adiabatic inspiral waveform ends when the orbital frequency reaches $f_{\rm ICO}$[2]. The quadrupole radiation frequency observed at the detector when the orbital frequency is $f_{\rm ICO}$ is

$$2f_{\rm max} = \frac{2f_{\rm ICO}}{1+z} \tag{3.7}$$

and the inspiral signal termination is represented in the detector response by the cut-off at $t > T'$ (see eqs. 3.4a and 3.6d).

Since the binary orbit evolves adiabatically from low frequencies to $f_{\rm ICO}$, the observed quadrupole radiation spectrum has significant power only up to frequency $2f_{\rm max}$. If $2f_{\rm max}$ is very much greater than the frequency where the detector noise is minimized, than the signal power bandwidth overlaps completely with the detector bandwidth and $\zeta(f_{\rm max}) \simeq 1$. On the other hand, if $2f_{\rm max}$ is much less than the frequency where the detector noise is minimized, than the overlap of the signal power and detector bandwidths is negligible, $\zeta(f_{\rm max}) \simeq 0$ and $\rho \simeq 0$.

The orbital frequency at the transition of the binary orbit from adiabatic inspiral to plunge and coalescence has been studied using high-order post-Newtonian methods [23]. For symmetric binaries (*i.e.,* those with equal-mass components) the instantaneous redshifted instantaneous orbital frequency of the ICO is given by

$$f_{\rm max} = \frac{f_{\rm ICO}}{1+z}, \tag{3.8a}$$

$$= \frac{710.\,{\rm Hz}}{1+z}\left(\frac{2.8\,{\rm M}_\odot}{M}\right), \tag{3.8b}$$

$$= \frac{99.\,{\rm Hz}}{1+z}\left(\frac{20.\,{\rm M}_\odot}{M}\right), \tag{3.8c}$$

where M is the binary's total mass. More generally, for binaries with compact components $f_{\rm ICO}$ depends inversely on M and directly on a function of the dimensionless ratio μ/M; Kidder [23, fig. 4] shows $Mf_{\rm ICO}$ for binary systems of arbitrary mass asymmetry. For a

---

[2]The radiation waveform from the final plunge and the early stages of coalescence is not yet known. If, after coalescence, a black hole forms, then the final radiation reflects the black hole's quasinormal modes, which are damped rapidly. The inspiral waveform, and with it our ability to model the detector response, ends when the orbital frequency reaches $f_{\rm ICO}$.

ns-ns binary the component's proper separation at the ICO is greater than a neutron star diameter; so, coalescence occurs after the transition from inspiral to plunge [23]. Tidal dissipation is important in determining the inspiral rate only in the last few orbits before contact [24,25]; consequently, equation 3.8 is applicable for ns-ns binaries and should be applicable for black hole binaries as well.

2. Detector bandwidth and data analysis templates

The probability that a signal with detector response $s(t)$ is present in the output $g(t)$ of a noisy detector is related to

$$2\,\langle g, s\rangle - \langle s, s\rangle\,, \tag{3.9a}$$

where

$$\langle g, h\rangle \equiv \int_{-\infty}^{\infty} df \frac{\widetilde{g}(f)\widetilde{h}^*(f)}{S_n(|f|)}. \tag{3.9b}$$

The actual signal, and consequently the detector response s, may be difficult or impossible to evaluate exactly (this is certainly the case for binary inspiral); so, we would like to be able to use an approximate model $S(t)$ in lieu of the actual detector response s in equations 3.9. From equations 3.9 it is clear that any approximate model $S(t)$ may be used as long as it matches $\widetilde{s}(f)$ closely wherever $|\widetilde{s}|^2/S_n(f)$ is relatively large. This latter quantity is just the fraction of ρ^2 contributed by the signal power at frequency f and is proportional to ζ'. This suggests that we define the *bandwidth function*

$$\mathcal{B}(f) \equiv \begin{cases} \frac{f}{2}\frac{\zeta'(f/2)}{\zeta(f_{\max})} & f < 2f_{\max} \\ 0 & f > 2f_{\max} \end{cases} \tag{3.10}$$

which is the fraction of the signal-to-noise ratio contributed by signal power at frequency f in a logarithmic frequency bandwidth. *An approximate detector response model $\widetilde{S}$ may be used instead of the actual response $\widetilde{s}$ as long as $\widetilde{S}$ accurately reflects $\widetilde{s}$ wherever $\mathcal{B}$ is large.* Knowing where and how $\widetilde{S}$ needs to be accurate can simplify greatly the construction of approximate templates for data analysis; for this purpose $\mathcal{B}$ should prove a useful guide.

E. Distribution of the orientation function Θ

The signal-to-noise ratio of an inspiraling binary in a single interferometric detector depends on the relative orientation of the source and the detector through the angles θ, ϕ, i, and ψ. The dependence of ρ on these angles is confined to the angular orientation function Θ, which is independent of all other properties of the binary system. From observations of binary inspiral in a single interferometer we can measure ρ and $\mathcal{M}$ but not Θ. Even though Θ cannot be measured, because it depends only on θ, ϕ, i and ψ we actually know quite a bit about it: since, averaged over many binaries, $\cos\theta$, ϕ/π, $\cos i$, and ψ/π are all uncorrelated and uniformly distributed over the range $(-1, 1)$ we know the probability that Θ takes on

any value. This probability distribution is found numerically in [4]; here I note only that $0 \leq \Theta \leq 4$ and that to an excellent approximation

$$P_\Theta(\Theta) = \begin{cases} 5\Theta\,(4-\Theta)^3\,/256 & \text{if } 0 < \Theta < 4 \\ 0 & \text{otherwise.} \end{cases} \tag{3.11}$$

To determine the binary coalescence rate ρ greater than ρ_0 we need to know $\mathcal{N}$ and also how the signal-to-noise ratio of binaries with intrinsic chirp mass $\mathcal{M}_0$ on a surface at redshift z is distributed. This latter distribution, $P_\rho(\rho|\mathcal{M}_0, z)$, is related to P_Θ:

$$\begin{aligned} P_\rho(\rho|\mathcal{M}_0, z, \mathcal{C}, \mathcal{D}) &= P_\Theta\left[\Theta(\rho)\right] \left.\frac{\partial\Theta}{\partial\rho}\right|_{\mathcal{M}_0,z} \\ &= P_\Theta\left[\frac{\rho}{8}\frac{d_L(z)}{r_0\,(1+z)^{5/6}}\left(\frac{1.2\,\mathrm{M}_\odot}{\mathcal{M}_0}\right)^{5/6}\right] \\ &\quad \times \frac{d_L\,(1.2\,\mathrm{M}_\odot/\mathcal{M}_0)^{5/6}}{8r_0\,(1+z)^{5/6}}, \end{aligned} \tag{3.12}$$

where $\mathcal{C}$ represents the cosmological model (H_0, q_0, Ω_0, $\mathcal{P}$, $\mathcal{E}$) and $\mathcal{D}$ the detector (*i.e.,* r_0 and ζ).

F. r_0 and ζ for the LIGO and VIRGO detectors

LIGO will consist of three interferometers: one in Livingston, Louisiana and two in Hanford, Washington. The Louisiana interferometer and one of the Washington interferometers will have 4 Km armlengths; the second Washington interferometer will have a 2 Km armlength and share the same vacuum system as the 4 Km interferometer. For the proposed LIGO interferometers as described in [26] and modeled in [4], r_0 ranges from 13 Mpc (for "initial" interferometers) to 237 Mpc (for "advanced" interferometers)[3]. As the LIGO detectors develop, incremental improvements will increase r_0.

The orientation of the Washington and Louisiana interferometers were chosen to be as close to parallel as possible; consequently, a simple approximation treats the LIGO *detector* (all three interferometers operating in "triple-coincidence") as a single interferometer of arm length

$$\left[4^2 + 4^2 + 2^2\right]^{1/2}\,\mathrm{Km} = 6\,\mathrm{Km}. \tag{3.13}$$

For this "super-interferometer" r_0 ranges from 19 Mpc to 355 Mpc.

---

[3]The noise model used in [26] and [4] assumed a thermal noise spectrum corresponding to viscous damping in the pendulum suspensions and the internal modes of the test masses. It is now recognized that these modes are structure damped [27–29] with a correspondingly different noise spectrum. Preliminary estimates indicate that this improved noise model reduces r_0 for initial LIGO interferometers, but leaves it unchanged for advanced ones.

Here and below, reference to the LIGO *detector* refers to the three interferometers operating as a single detector, while reference to a LIGO *interferometer* indicates one of the 4 Km interferometers operating in isolation.

Figure 1 shows ζ for early LIGO and VIRGO interferometers and also more advanced LIGO interferometers as have been discussed in the literature [26,4]. The solid curve shows ζ representative of advanced interferometers, while the dashed and dotted curves show ζ representative of initial LIGO and VIRGO interferometers. As the LIGO detector evolves, r_0 will increase from approximately 20 Mpc toward 350 Mpc, and ζ will evolve from the dashed curve toward the solid curve. Setting aside the overall sensitivity gain with increasing r_0, the evolution of ζ signifies an increasing *relative* sensitivity to systems with small $f_{\rm max}$: *i.e.,* systems with larger total masses and/or redshifts.

VIRGO will consist of a single 3 Km interferometer. The target noise curve for the initial operation of the VIRGO interferometer is described in [2]; for this interferometer r_0 is 13 Mpc. Like the LIGO interferometers, incremental improvements in VIRGO will increase r_0 and it is reasonable to assume that these improvements could raise r_0 for VIRGO to approximately 200 Mpc. The dotted curve in figure 1 shows ζ for the initial VIRGO interferometers. Note how, even though r_0 is the same for both the initial LIGO and VIRGO interferometers, the relative sensitivity of these two detectors to signals at low and high frequency — corresponding to more or less massive binaries — is markedly different. Improvements in the VIRGO interferometer can be expected to evolve ζ toward the solid curve as well. Note that the initial VIRGO interferometers are expected to be relatively more sensitive to massive (*i.e.,* low $f_{\rm max}$) binaries than are the initial LIGO interferometers.

For neutron star binaries $f_{\rm max} \simeq 710\,{\rm Hz}$ (eq. 3.8) and $\zeta(f_{\rm max}) \simeq 1$ in any of the proposed LIGO and VIRGO interferometers (see fig. 1). Figure 2 shows the bandwidth function for neutron star binary observations in early VIRGO (dotted curve) and LIGO (dashed curve) interferometers and also more advanced LIGO interferometers (solid curve). It is clear that the approximate detector response models for binary inspiral observations must evolve with the interferometers: in the early interferometers the detector response models will need to be quite accurate at high frequencies ($f \simeq 200\,{\rm Hz}$) but not at low ones; on the other hand, in more advanced interferometers these models will need to be accurate at low frequencies ($f \simeq 60\,{\rm Hz}$) and, to obtain this low frequency accuracy, the high frequency performance may be sacrificed at no cost to the signal detectability.

IV. DISCUSSION

A. Introduction

Consider a catalog of binary inspiral events with signal-to-noise ratio ρ greater than a threshold ρ_0. Suppose that for each event in the catalog ρ and $\mathcal{M}$ are known. How do we make use of the catalog to test cosmological models against cataloged observations?

The simplest test involves the distribution of events with ρ. As the catalog limit ρ_0 decreases, sources at increasingly larger distance become members. The number of added sources depends on the increase of the spatial volume, the density of sources at that distance, and (since these sources are *events* that occur at a given *rate*) the cosmological redshift.

Thus, adopting a cosmological model $\mathcal{C}$ implies an expected distribution $P(\rho|\rho_0, \mathcal{C}, \mathcal{D})$ for the catalog events taken with detector $\mathcal{D}$. Denote the cataloged binary inspiral signal-to-noise ratio observations by $\{\rho|\rho > \rho_0\}$. Suppose that, before studying these observations, we have reason or are otherwise prejudiced to believe the probability that $\mathcal{C}$ is the correct cosmological model is $P(\mathcal{C})$. Using Bayes' law of conditional probabilities, the *a posteriori* probability that we assign to model $\mathcal{C}$ after considering the observations is

$$P(\mathcal{C}|\{\rho|\rho > \rho_0\}) \propto P(\mathcal{C}) \prod_i P(\rho_i|\rho_0, \mathcal{C}, \mathcal{D}_i), \tag{4.1}$$

where ρ_i is the signal-to-noise ratio of the i^{th} catalog observation and $\mathcal{D}_i$ represents the detector configuration (r_0, ζ) when the observation was made[4]. This test is exactly analogous to number-flux cosmological tests using distant galaxies.

More subtle tests involve other distributions of cataloged events. For example, each source in the catalog is characterized by its observed chirp mass $\mathcal{M}$. The observed chirp mass depends on both the intrinsic chirp mass $\mathcal{M}_0$ and the redshift z (see eq. 2.2); consequently, the distribution of events in the catalog with $\mathcal{M}$ depends on the cosmological model. Denote the cataloged chirp mass observations by $\{\mathcal{M}|\rho > \rho_0\}$. Adopting a cosmological model $\mathcal{C}$ implies an expected distribution $P(\mathcal{M}|\rho_0, \mathcal{C}, \mathcal{D})$. As before, if we initially favor model $\mathcal{C}$ with probability $P(\mathcal{C})$, then after studying the observations the probability we ascribe to model $\mathcal{C}$ is

$$P(\mathcal{C}|\{\mathcal{M}|\rho > \rho_0\}) \propto P(\mathcal{C}) \prod_i P(\mathcal{M}_i|\rho_0, \mathcal{C}, \mathcal{D}_i), \tag{4.2}$$

where $\mathcal{M}_i$ represents the i^{th} cataloged chirp mass observation.

Of the four parameters that describe, at quadrupole order, binary inspiral observed in a single interferometer, only ρ and $\mathcal{M}$ convey astrophysically interesting information. The distributions $P(\rho|\rho_0, \mathcal{C}, \mathcal{D})$ and $P(\mathcal{M}|\rho_0, \mathcal{C}, \mathcal{D})$ are each integrals over the distribution $P(\rho, \mathcal{M}|\rho_0, \mathcal{C}, \mathcal{D})$ that completely characterizes the catalog:

$$P(\rho|\rho_0, \mathcal{C}, \mathcal{D}) = \int P(\rho, \mathcal{M}|\rho_0, \mathcal{C}, \mathcal{D}) d\mathcal{M} \tag{4.3a}$$

$$P(\mathcal{M}|\rho_0, \mathcal{C}, \mathcal{D}) = \int_{\rho_0}^{\infty} P(\rho, \mathcal{M}|\rho_0, \mathcal{C}, \mathcal{D}) d\rho. \tag{4.3b}$$

These integrals are *summaries* of the catalog contents: as such, they are less informative than $P(\rho, \mathcal{M}|\rho_0, \mathcal{C}, \mathcal{D})$. The most sensitive test that we can make using the catalog involves not a summary, but the full information available: given the observations $\{\rho, \mathcal{M}|\rho > \rho_0\}$, the probability that cosmological model $\mathcal{C}$ describes our universe is

---

[4]Changes in the detector noise spectrum change the relation between ρ and the cosmological model. This is not a problem in the interpretation of a catalog as long as the detector properties are properly associated with each cataloged observation.

$$P(\mathcal{C}|\{\rho,\mathcal{M}\},\rho_0) \propto P(\mathcal{C})\prod_i P(\rho_i,\mathcal{M}_i|\rho_0,\mathcal{C},\mathcal{D}_i). \tag{4.4}$$

Cosmological tests based on the summary distributions are still useful to make. Summary distribution often depend only weakly or not at all on some of the parameters of the model $\mathcal{C}$; in that case, the effective dimensionality of $\mathcal{C}$ is reduced in the summary test and we may be able to distinguish more closely among cosmological models described by the remaining parameters than with a test using the full distribution. This is particularly true when the number of observations in the catalog is small.

B. Outline

In this section I give general expressions for the distributions $P(\rho,\mathcal{M}|\rho_0,\mathcal{C},\mathcal{D})$ and the summary distributions $P(\rho|\rho_0,\mathcal{C},\mathcal{D})$ and $P(\mathcal{M}|\rho_0,\mathcal{C},\mathcal{D})$ that can be evaluated in any homogeneous and isotropic cosmological model; in addition, I evaluate the summary distributions explicitly for matter-dominated Friedmann-Robertson-Walker (FRW) models. The essential properties of FRW cosmological models are summarized in section IV C.

In addition to the distributions $P(\rho,\mathcal{M}|\rho_0,\mathcal{C},\mathcal{D})$, $P(\rho|\rho_0,\mathcal{C},\mathcal{D})$ and $P(\mathcal{M}|\rho_0,\mathcal{C},\mathcal{D})$ are other catalog properties of intrinsic interest. In a given cosmological model there is a distance beyond which no binary inspiral of fixed intrinsic chirp mass will have signal-to-noise ratio greater than the catalog limit ρ_0, and I calculate this *catalog depth* z_0 in section IV D. A catalog takes time to build, and, in a given period of time, the size of a binary inspiral catalog is limited by the rate dN/dt at which binaries coalesce with ρ greater than the catalog threshold ρ_0. In section IV E I calculate both the expected rate of binary inspiral observations and the distribution $P(\rho|\rho_0,\mathcal{C},\mathcal{D})$ for advanced LIGO interferometers and describe how these depend on the cosmological model $\mathcal{C}$. Finally, in section IV F I calculate the distribution $P(\mathcal{M}|\rho_0,\mathcal{C},\mathcal{D})$ and describe how it depends on $\mathcal{C}$.

C. Cosmological model

Specific examples of the catalog distributions, catalog depth, and rate of binary inspiral observations made in this section are in the context of matter-dominated Friedmann-Robertson-Walker (FRW) cosmological models. The Robertson-Walker spacetime metric has the line element

$$ds^2 = -dt^2 + a^2(t)\left[\frac{dr^2}{1-kr^2} + r^2\left(d\theta^2 + \sin^2\theta d\phi^2\right)\right], \tag{4.5}$$

where $a(t)$ is the usual (dimensioned) scale factor, r is a dimensionless parameter related to the area of spheres of constant radius, and k is $+1$, -1, or 0 depending on whether the spatial geometry of the slices of homogeneity has positive, negative, or zero curvature (*i.e.,* is closed, open, or flat). In matter dominated FRW models (which have vanishing cosmological constant) the co-moving radial coordinate r and the luminosity distance d_L can be written in terms of the redshift explicitly:

$$r = \frac{z q_0 + (q_0 - 1)\left[(1 + 2q_0 z)^{1/2} - 1\right]}{a_0 H_0 q_0^2 (1+z)}, \tag{4.6a}$$

$$d_L = a_0 (1+z)\, r, \tag{4.6b}$$

where a_0, H_0, and q_0 are the scale factor, expansion rate, and curvature parameter (deceleration parameter) at the present epoch [30, eq. 15.3.24].

D. Sample depth

The signal-to-noise ratio of an inspiraling neutron star binary system with intrinsic chirp mass $\mathcal{M}_0$ is

$$\rho = 8\Theta \left(\frac{r_0}{d_L}\right) \left(\frac{\mathcal{M}_0}{1.2\mathrm{M}_\odot}\right)^{5/6} (1+z)^{5/6}\, \zeta(f_{\max}). \tag{4.7}$$

Since Θ is between 0 and 4, even an optimally oriented binary system has ρ less than ρ_0 when z is greater than z_0, where z_0 satisfies

$$4 = \frac{\rho_0 d_L(z_0)}{8 r_0 \zeta(f_{\max})^{5/6}} \left(\frac{1.2\,\mathrm{M}_\odot}{\mathcal{M}_0}\right)^{5/6}. \tag{4.8}$$

Evaluation of z_0 requires $\zeta(f_{\max})$, which depends on the details of the detector's noise power spectral density (through ζ) as well as the binary's component masses and redshift (through $f_{\max}$). For advanced interferometers $\zeta \simeq 1$ as long as $f_{\max} \gtrsim 70\,\mathrm{Hz}$ (see fig. 1) while $f_{\max} \simeq 710\,\mathrm{Hz}\,[2.8\,\mathrm{M}_\odot/(1+z_0)M]$ for symmetric binary inspiral (see eq. 3.8). Consequently, we can approximate $\zeta \simeq 1$ as long as $1 + z_0 \lesssim 10\,(2.8\,\mathrm{M}_\odot/M)$. For small z_0 we can approximate $d_L \simeq z/H_0$; then

$$z_0 \simeq \frac{32 H_0 r_0}{\rho_0} \left(\frac{\mathcal{M}_0}{1.2\,\mathrm{M}_\odot}\right)^{5/6} \tag{4.9a}$$

$$\simeq 0.48 h \left(\frac{8}{\rho_0}\right) \left(\frac{r_0}{355\,\mathrm{Mpc}}\right) \left(\frac{\mathcal{M}_0}{1.2\,\mathrm{M}_\odot}\right)^{5/6}, \tag{4.9b}$$

which is much less than 10. Thus, the approximation $\zeta \simeq 1$ is a good one for binary systems with solar mass components, but not for binaries whose components are on order $5\,\mathrm{M}_\odot$.

For a specific example, focus attention first on solar mass component binaries. Then $\zeta \simeq 1$ for any of the proposed LIGO or VIRGO interferometers (at the end of this subsection I return to consider briefly the case of more massive binary systems where this is not true). In an Einstein-deSitter ($q_0 = 1/2$) cosmological model z_0 is then given explicitly by

$$z_0 = \left[\beta + \frac{256}{9\beta}\alpha_0^2 + \frac{16}{3}\alpha_0\right]^6 - 1, \tag{4.10a}$$

where

$$\alpha_0 = \frac{8H_0 r_0}{\rho_0}\left(\frac{\mathcal{M}_0}{1.2\,\mathrm{M}_\odot}\right)^{5/6} \tag{4.10b}$$

$$= 0.12h\left(\frac{8}{\rho_0}\right)\left(\frac{r_0}{355\,\mathrm{Mpc}}\right)\left(\frac{\mathcal{M}_0}{1.2\,\mathrm{M}_\odot}\right)^{5/6}, \tag{4.10c}$$

h is the Hubble parameter (H_0 in units of 100 Km/s/Mpc), and

$$\beta = \left[\frac{1}{2} + \left(\frac{16\alpha_0}{3}\right)^3 + \left(\frac{1}{4} + \frac{4096}{27}\alpha_0^3\right)^{1/2}\right]^{1/3}. \tag{4.10d}$$

More generally ($q_0 \neq 1/2$ but ζ still unity) z_0 satisfies

$$z_0 = x^6 - 1 \tag{4.11a}$$

where x is a root of

$$0 = x^{12} + 8q_0\alpha_0 x^{11} + 16q_0^2\alpha_0^2 x^{10} - 2q_0 x^6 - 8\alpha_0(2q_0 - 1)x^5 + 2q_0 - 1. \tag{4.11b}$$

The appropriate root of this equation can be found as a power series for small α_0:

$$z_0 = 4\alpha_0 + \frac{8}{3}\left(3q_0 + 2\right)\alpha_0^2 + 8\left(6q_0 - 1\right)\alpha_0^3 + \frac{160}{81}\left(54q_0^2 + 9q_0 - 7\right)\alpha_0^4 + \frac{5600}{243}\left(27q_0^2 - \frac{447}{25}q_0 + \frac{323}{100}\right)\alpha_0^5 + \mathcal{O}(\alpha_0^6) \tag{4.12}$$

This truncated expansion is accurate to better than 0.2% for $\alpha_0 < 0.12$ and $0 \leq q_0 \leq 1$; for $\alpha_0 < 0.1$ and $0 \lesssim q_0 \lesssim 3/4$ the accuracy is better than 0.01%. An asymptotic expansion for z_0 valid for large α_0 (but ζ still 1) is

$$z_0 = 4096q_0^6\alpha_0^6 - 384\sqrt{2q_0^5}\left(q_0 - 1\right)\alpha_0^3 + 6q_0 - 1 + \mathcal{O}\left(\alpha_0^{-3}\right). \tag{4.13}$$

This asymptotic expansion is accurate to better than 1% for $\alpha_0 \gtrsim 1/2$ and $0.1 \lesssim q_0 \lesssim 1$.

Figure 3 shows z_0 as a function of h for neutron star binaries with $\mathcal{M}_0 = 1.19\,\mathrm{M}_\odot$ (corresponding to $1.37\,\mathrm{M}_\odot$ neutron stars), $\rho_0 = 8$, $r_0 = 355$, and three different values of q_0 corresponding to an open ($q_0 = 1/4$, dotted curve), flat ($q_0 = 1/2$, solid curve) and closed ($q_0 = 3/4$, dashed curve) cosmological model. The redshift of the most distant such source is less than 1/2 for $h < 0.8$ and does not exceed 7/10 for $h < 1$. The sensitivity of z_0 to q_0 is modest but significant: inspection of equation 4.11 shows that

$$z_0 \simeq 4\alpha_0\left[1 + \alpha_0\left(2q_0 - 1\right)\right] + \mathcal{O}\left[\alpha_0^3, \left(2q_0 - 1\right)^2\right], \tag{4.14}$$

where $\alpha_0 \simeq 0.12h$ for advanced LIGO interferometers. For open spatial geometries ($2q_0 - 1 < 0$) the most distant sources are at smaller redshifts than in closed spatial geometries (where $2q_0 - 1 > 0$).

In luminosity distance, the sample depth is

$$d_{L,0} = \frac{4\alpha_0}{H_0}\left[1 + \frac{40}{3}\alpha_0 + \frac{40}{3}\left(2q_0+1\right)\alpha_0^2 + \frac{1280}{81}\left(9q_0-2\right)\alpha_0^3 \right.$$
$$\left. + \frac{40}{243}\left(2052q_0^2 - 180q_0 - 143\right)\alpha_0^4 + \mathcal{O}\left(\alpha_0^6\right)\right]. \tag{4.15}$$

Figure 4 shows $d_{L,0}$ for the same cases (h, q_0) as figure 3 shows z_0. Advanced LIGO interferometers may observe neutron star binaries with ρ greater than 8 at luminosity distances of order 2 Gpc.

For more massive binaries $\zeta(f_{\max})$ is substantially less than unity at z_0 and the approximation $\zeta \simeq 1$ is no longer valid. Figure 5 shows z_0 (given implicitly by eq. 4.8) for an advanced LIGO detector ($r_0 = 355\,\mathrm{Mpc}$) and a range of binary systems in two distinct Einstein-de Sitter ($q_0 = 1/2$) cosmological models. One pair of curves show z_0 for symmetric binaries consisting of two (*e.g.*) black holes each of mass $M_{\rm bh}$, while the second pair of curves shows z_0 for asymmetric binaries, consisting of (*e.g.,*) a black hole of mass $M_{\rm bh}$ and a neutron star of mass $1.4\,\mathrm{M}_\odot$. Note how, in *all* cases, z_0 does not increase without bound as $M_{\rm bh}$ increases; instead, it has a maximum value for some $M_{\rm bh}$ and decreases as $M_{\rm bh}$ increases further.

The finite bandwidth of the detector and its overlap with the signal power, as represented by ζ, determines the maximum redshift at which a detector can observe binary inspiral. If ζ were constant then z_0 would increase monotonically with $\mathcal{M}_0$ (see eq. 4.8); however, ζ is not constant and as $\mathcal{M}$ increases $f_{\max}$ decreases both because $f_{\rm ICO}$ is decreasing and also because z_0 is increasing ($f_{\max} \propto M/(1+z)$; see eq. 3.8). Eventually ζ begins to decrease with increasing $\mathcal{M}_0$ or decreasing $f_{\max}$ (for advanced LIGO interferometers, ζ remains unity until $f_{\max} \simeq 70\,\mathrm{Hz}$; see fig. 1). Once ζ begins to decrease so to will z_0. For sufficiently large $\mathcal{M}_0$ even a local binary ($z = 0$) will coalesce before the gravitational radiation signal enters the detector bandwidth.

Thus, decreasing the detector noise at low frequencies has a dual effect: by increasing r_0 it increases the overall detector sensitivity, and by decreasing the frequency below which $\zeta \ll 1$ it further boosts the sensitivity of the interferometer to more massive and more distant binary systems. Advanced LIGO detectors are expected to be most sensitive to inspiraling binaries with two $10\,\mathrm{M}_\odot$ black hole components, which will be observable with ρ greater than 8 at redshifts greater than 1.5.

E. Coalescence rate above threshold

The distribution of catalog events with ρ is given by

$$P(\rho|\rho_0, \mathcal{C}, \mathcal{D}) = \begin{cases} \frac{d^2N/dt\,d\rho}{dN/dt} & \rho > \rho_0, \\ 0 & \rho < \rho_0, \end{cases} \tag{4.16a}$$

where

$$\frac{d^2N}{dt\,d\rho} = \int d\mathcal{M}_0 \frac{d^3N}{dt\,d\rho\,d\mathcal{M}_0}, \tag{4.16b}$$

$$\frac{d^3N}{dt\,d\rho\,d\mathcal{M}_0} = \int dz \frac{dr}{dz}\frac{4\pi a_0^3 r^2}{\sqrt{1-kr^2}}\frac{\dot{n}_0\mathcal{E}(z)}{1+z} \times \frac{\mathcal{P}\left(\mathcal{M}_0|z\right)}{1+z} P_\rho(\rho|z,\mathcal{M}_0,\mathcal{C},\mathcal{D}), \tag{4.16c}$$

$$\frac{dN}{dt} = \int_{\rho_0}^{\infty} d\rho\,\frac{d^2N}{dt\,d\rho}, \tag{4.16d}$$

and P_ρ is given in equation 3.12.

Since $d^2N/dt\,d\rho$ depends on ρ only through P_ρ, the integral over ρ in equation 4.16d can be evaluated explicitly. First note that

$$\int_{\rho_0}^{\infty} d\rho\, P_\rho(\rho|\mathcal{M}_0,z,\mathcal{C},\mathcal{D}) = \int_x^{\infty} P_\Theta(\Theta) \tag{4.17a}$$

$$\equiv C_\Theta(x), \tag{4.17b}$$

where

$$x = \frac{\rho_0}{8}\frac{d_L}{r_0\left(1+z\right)^{5/6}}\left(\frac{1.2\,\mathrm{M}_\odot}{\mathcal{M}_0}\right)^{5/6}. \tag{4.17c}$$

The probability density P_ρ is a conditional one: it depends on $\mathcal{M}_0$, z, and the cosmological model. In contrast, the distribution P_Θ of Θ is universal: it is independent of all the specific properties of the binary or the detector. $C_\Theta(x)$ is universal in this same way and can be evaluated with P_Θ. In terms of C_Θ the total rate of inspirals with ρ greater than ρ_0 is

$$\frac{dN}{dt} = \int d\mathcal{M}_0 \frac{d^2N}{dt\,d\mathcal{M}_0}, \tag{4.18a}$$

where

$$\frac{d^2N}{dt\,d\mathcal{M}_0} = \int_0^{\infty} dz\,\frac{dr}{dz}\frac{4\pi a_0^3 r^2}{\sqrt{1-kr^2}}\frac{\dot{n}_0\mathcal{E}(z)}{1+z}\mathcal{P}\left(\mathcal{M}_0|z\right) \times C_\Theta\left[\frac{d_L(z)}{\alpha_0\left(1+z\right)^{5/6}\zeta(f_{\max})}\right] \tag{4.18b}$$

and

$$\alpha_0 \equiv \frac{8H_0 r_0}{\rho_0}\left(\frac{\mathcal{M}_0}{1.2\,\mathrm{M}_\odot}\right)^{5/6}. \tag{4.18c}$$

Equation 4.18 for dN/dt, which is also the total rate of binary inspiral with $\rho > \rho_0$, and equations 4.16 for $P(\rho|\rho_0,\mathcal{C},\mathcal{D})$ are valid for any homogeneous and isotropic cosmological model.

1. Examples: Constant $\mathcal{M}_0$

Turn now to the specific example of neutron star binaries in matter-dominated FRW cosmological models, so that $\zeta \simeq 1$ and r and d_L are given by equations 4.6. Assume also that evolution in the binary population is unimportant over redshifts $z \lesssim 1/2$; then $\mathcal{E}$ is unity and $\mathcal{P}$ is independent of z. Finally, use the approximation given above for P_Θ (eq. 3.11) to evaluate C_Θ:

$$C_\Theta(x) \simeq \begin{cases} 1 & \text{if } x \leq 0 \\ (1+x)(4-x)^4/256 & \text{if } 0 \leq x \leq 4 \\ 0 & \text{if } 4 < x. \end{cases} \tag{4.19}$$

The integral for $d^2N/dt\,d\mathcal{M}_0$ (eq. 4.18b) can then be evaluated as a power series in small α_0:

$$\frac{d^2N}{dt\,d\mathcal{M}_0} = \left(\frac{dN}{dt}\right)_0 \mathcal{P}(\mathcal{M}_0) \tag{4.20a}$$

where

$$\left(\frac{dN}{dt}\right)_0 = \left(\frac{128}{21}\pi r_0^3 \dot{n}_0\right)\left(\frac{8}{\rho_0}\right)^3 \left(\frac{\mathcal{M}_0}{1.2\mathrm{M}_\odot}\right)^{5/2} \left[1 - \frac{25}{9}\alpha_0 + \frac{2}{45}\left(6q_0+85\right)\alpha_0^2 - \frac{224}{33}q_0\alpha_0^3 + \frac{20}{8019}\left(1188q_0^2+9108q_0-4123\right)\alpha_0^4 + \mathcal{O}\left(\alpha_0^5\right)\right] \tag{4.20b}$$

and α_0 is given by equation 4.10b. Similarly, $d^3N/dt\,d\rho\,d\mathcal{M}_0$ is given by

$$\frac{d^3N}{dt\,d\rho\,d\mathcal{M}_0} = \left(\frac{d^2N}{dt\,d\rho}\right)_0 \mathcal{P}(\mathcal{M}_0) \tag{4.21a}$$

where

$$\left(\frac{d^2N}{dt\,d\rho}\right)_0 = \left(\frac{16}{7}\pi r_0^3 \dot{n}_0\right)\left(\frac{8}{\rho}\right)^4 \left(\frac{\mathcal{M}_0}{1.2\mathrm{M}_\odot}\right)^{5/2} \left[1 - \frac{100}{27}\alpha + \frac{2}{27}\left(6q_0+85\right)\alpha^2 - \frac{448}{33}q_0\alpha^3 + \frac{140}{24057}\left(1188q_0^2+9108q_0-4123\right)\alpha^4 + \mathcal{O}\left(\alpha^5\right)\right] \tag{4.21b}$$

and

$$\begin{aligned} \alpha &= \frac{8H_0 r_0}{\rho}\left(\frac{\mathcal{M}_0}{1.2\,\mathrm{M}_\odot}\right)^{5/6} \\ &= \alpha_0\left(\frac{\rho_0}{\rho}\right). \end{aligned} \tag{4.21c}$$

Equations 4.20 and 4.21 for $d^2N/dt\,d\mathcal{M}_0$ and $d^3N/dt\,d\rho\,d\mathcal{M}_0$ can be integrated over $\mathcal{M}_0$ to find dN/dt and $d^2N/dt\,d\rho$, and thus $P(\rho|\rho_0, \mathcal{C}, \mathcal{D})$.

Observational and theoretical evidence suggests that the ns-ns binary intrinsic chirp mass distribution is sharply peaked (see sec. II C). In the most extreme limit that all binary systems have intrinsic chirp mass $\mathcal{M}_0$, $\mathcal{P}$ is a δ-function in $\mathcal{M}_0$ and

$$\frac{dN}{dt} = \left(\frac{dN}{dt}\right)_0 \tag{4.22a}$$

$$\begin{aligned} P(\rho|\rho_0,\mathcal{C},\mathcal{D}) &= \frac{(d^2N/dt\,d\rho)_0}{(dN/dt)_0} \\ &= \frac{3}{\rho}\left(\frac{\rho_0}{\rho}\right)^3 \frac{\begin{array}{c}1-\frac{100}{27}\alpha+\frac{2}{27}\left(6q_0+85\right)\alpha^2-\frac{448}{33}q_0\alpha^3 \\ +\frac{140}{24057}\left(1188q_0^2+9108q_0-4123\right)\alpha^4\end{array}}{\begin{array}{c}1-\frac{25}{9}\alpha_0+\frac{2}{45}\left(6q_0+85\right)\alpha_0^2-\frac{224}{33}q_0\alpha_0^3 \\ +\frac{20}{8019}\left(1188q_0^2+9108q_0-4123\right)\alpha_0^4\end{array}} + \mathcal{O}\left(\alpha_0^5,\alpha^5\right). \end{aligned} \tag{4.22b}$$

Figure 6 shows $(dN/dt)_0$ as a function of h in an Einstein-deSitter cosmological model ($q_0 = 1/2$) for a reasonable signal-to-noise ratio limit in an advanced LIGO detector ($\rho_0 = 8$ and $r_0 = 355\,\mathrm{Mpc}$), typical neutron star masses ($\mathcal{M}_0 = 1.19\,\mathrm{M}_\odot$), and two different coalescence rate densities. The solid curve shows $(dN/dt)_0$ for the "best guess" coalescence rate density, $\dot{n}_0 = 1.1\times10^{-7}h\,\mathrm{Mpc}^{-3}\,\mathrm{s}^{-1}$ (see sec. II C 1), which is proportional to h; the dashed curve shows $(dN/dt)_0$ for a constant coalescence rate density $\dot{n}_0 = 8\times10^{-8}\,\mathrm{Mpc}^{-1}\,\mathrm{yr}^{-1}$. The dashed curve shows how $(dN/dt)_0$ scales for constant $\dot{n}_0$ in advanced interferometers with interesting h. Present estimates of $\dot{n}_0$ suggest that, if $h = 0.75$, advanced LIGO detectors can expect to observe a little more than 1 neutron star binary inspiral event per week.

The distribution $P(\rho|\rho_0,\mathcal{C},\mathcal{D})$ is also sensitive to h. Let $\mathcal{C}_0$ represent a flat and static cosmological model. Then

$$P(\rho|\rho_0,\mathcal{C}_0,\mathcal{D}) = \begin{cases} 3\rho_0^3/\rho^4 & \rho > \rho_0 \\ 0 & \rho < \rho_0 \end{cases} \tag{4.23}$$

The first order correction (in $1/\rho$) owing to the expansion of the universe depends only on the rate of expansion (H_0); corrections owing to the curvature of space ($k \neq 0$) enter only at second order in $1/\rho$. Since, for ns-ns binaries and reasonable limiting signal-to-noise α^2 is less than 1% even for advanced interferometer designs, cosmological tests that focus only on the observed distribution of ρ will be insensitive to q_0 even though the redshift to the most distant sources in the catalog is large (this weak dependence on q_0 is characteristic of number-flux cosmological tests (see, *e.g.,* [31, pg. 798]). On the other hand, for advanced detectors and interesting cosmological models, the distribution $P(\rho|\rho_0,\mathcal{C},\mathcal{D})$ is sensitive to h at the 10% level, which makes possible a measurement of h from the observations $\{\rho|\rho > \rho_0\}$ alone. Figure 7 shows $P(\rho|\rho_0,\mathcal{I})/P(\rho|\rho_0,\mathcal{C}_0,\mathcal{D})$ for two Einstein-deSitter cosmological models that differ only by h (in both cases $\mathcal{M}_0 = 1.19\,\mathrm{M}_\odot$). The general trend is that with increasing h inspiral events are shifted toward larger ρ compared to the distribution in a static universe.

2. Examples: Uniformly distributed neutron star masses

In a less extreme limit assume that neutron star masses are bounded above by m_h and below by m_l, that between these bounds their masses are uniformly distributed, and that

the component masses of an inspiraling binary system are uncorrelated. Then $\mathcal{P}(\mathcal{M}_0)$ is given approximately by equation 2.14, and

$$\frac{d^2N}{dt\,d\rho} = \left(\frac{16}{7}\pi r_0^3 \dot{n}_0\right)\left(\frac{8}{\rho}\right)^4\left(\frac{m_0}{1.2\mathrm{M}_\odot}\right)^{5/2}\left[\xi_{5/2} - \frac{100}{27}\bar{\alpha}\xi_{10/3} + \frac{2}{27}\left(6q_0+85\right)\bar{\alpha}^2\xi_{25/6} - \frac{448}{33}q_0\bar{\alpha}^3\xi_5 + \frac{140}{24057}\left(1188q_0^2+9108q_0-4123\right)\bar{\alpha}^4\xi_{35/6} + \mathcal{O}\left(\bar{\alpha}^5\right)\right] \tag{4.24a}$$

$$\frac{dN}{dt} = \left(\frac{128}{21}\pi r_0^3 \dot{n}_0\right)\left(\frac{8}{\rho_0}\right)^3\left(\frac{m_0}{1.2\mathrm{M}_\odot}\right)^{5/2}\left[\xi_{5/2} - \frac{25}{9}\bar{\alpha}_0\xi_{10/3} + \frac{2}{45}\left(6q_0+85\right)\bar{\alpha}_0^2\xi_{25/6} - \frac{224}{33}q_0\bar{\alpha}_0^3\xi_5 + \frac{20}{8019}\left(1188q_0^2+9108q_0-4123\right)\bar{\alpha}_0^4\xi_{35/6} + \mathcal{O}\left(\bar{\alpha}_0^5\right)\right] \tag{4.24b}$$

where

$$\xi_n(x_h, x_l) = \frac{2\left[x_h^{n+2}\left(1-x_l\right) + x_l^{n+2}\left(x_h-1\right) - \left(x_h - x_l\right)\right]}{\left(n+2\right)\left(n+1\right)\left(x_h-x_l\right)\left(x_h-1\right)\left(1-x_l\right)} \tag{4.24c}$$

and

$$\bar{\alpha} = \left(\frac{8H_0 r_0}{\rho}\right)\left(\frac{m_0}{1.2\,\mathrm{M}_\odot}\right)^{5/6} \tag{4.24d}$$

$$\bar{\alpha}_0 = \left(\frac{8H_0 r_0}{\rho_0}\right)\left(\frac{m_0}{1.2\,\mathrm{M}_\odot}\right)^{5/6} \tag{4.24e}$$

$$x_h = \frac{m_>}{m_0} \tag{4.24f}$$

$$x_l = \frac{m_<}{m_0} \tag{4.24g}$$

$$m_< = m_l/2^{1/5} \tag{4.24h}$$

$$m_0 = \left(m_l m_h\right)^{3/5}/\left(m_l+m_h\right)^{1/5} \tag{4.24i}$$

$$m_> = m_h/2^{1/5}. \tag{4.24j}$$

Over the range of $\bar{\alpha}_0$ relevant for neutron star binary inspiral observations in LIGO-like interferometric detectors, dN/dt and $d^2N/dt\,d\rho$ are only weakly dependent on m_l and m_h for constant m_0: taking

$$x_l = 1-\epsilon \tag{4.25a}$$

we find

$$x_h = 1+\epsilon+\frac{6}{5}\epsilon^2+\frac{36}{25}\epsilon^3 + \frac{42}{25}\epsilon^4+\frac{1188}{625}\epsilon^5+\mathcal{O}(\epsilon^6) \tag{4.25b}$$

$$\frac{dN}{dt}(\epsilon) = \frac{dN}{dt}(0)\left[1+\frac{21}{16}\epsilon^2+\mathcal{O}\left(\alpha,\epsilon^3\right)\right]. \tag{4.25c}$$

Observations suggest that ϵ is small [20], in which case the distribution of ρ in LIGO observations is insensitive to the finite neutron star mass range.

F. Chirp mass spectrum $P(\mathcal{M}|\rho_0, \mathcal{I})$

In a homogeneous and isotropic cosmology the rate at which binary inspiral signals corresponding to chirp mass $\mathcal{M}$ and ρ greater than ρ_0 are observed is

$$\frac{d^2N}{dt\,d\mathcal{M}} = \int_0^\infty dz\,\frac{dr}{dz}\frac{4\pi a_0^3 r^2}{(1-kr^2)^{1/2}}\frac{\dot{n}_0\mathcal{E}(z)}{1+z}\frac{\mathcal{P}\left(\frac{\mathcal{M}}{1+z}|z\right)}{1+z}C_\Theta\left[\frac{\rho_0}{8}\frac{d_L}{r_0\zeta(f_{\max})}\left(\frac{1.2\,\mathrm{M}_\odot}{\mathcal{M}}\right)^{5/6}\right]. \quad (4.26)$$

The catalog's *a priori* chirp mass distribution is thus

$$P(\mathcal{M}|\rho_0, \mathcal{C}, \mathcal{D}) = \frac{d^2N/dt\,d\mathcal{M}}{dN/dt} \quad (4.27)$$

where dN/dt is given by equation 4.16d and $\mathcal{C}$ represents assumptions regarding the cosmology (H_0, q_0, Ω_0), evolution and the distribution of neutron star masses ($\mathcal{E}$, $\mathcal{P}$), and other, unenumerated, model assumptions.

As discussed in section II C, observational and theoretical evidence suggest that the ns-ns binary intrinsic chirp mass distribution is sharply peaked. Neglecting evolution and taking the intrinsic chirp mass of all binary systems to be a constant $\mathcal{M}_0$,

$$\frac{d^2N}{dt\,d\mathcal{M}} = \frac{\dot{n}_0\mathcal{E}(Z)}{\mathcal{M}}\frac{dr}{dz}(Z)\frac{4\pi a_0^3 r^2(Z)}{\sqrt{1-kr^2(Z)}}C_\Theta\left[\frac{\rho_0}{8}\frac{d_L(Z)}{(1+Z)^{5/6}r_0}\left(\frac{1.2\,\mathrm{M}_\odot}{\mathcal{M}_0}\right)^{5/6}\right], \quad (4.28)$$

where

$$Z = \frac{\mathcal{M}}{\mathcal{M}_0} - 1. \quad (4.29)$$

Figure 8 shows the distribution $P(\mathcal{M}|\rho_0, \mathcal{C}, \mathcal{D})$ for catalogs with ρ greater than 8 compiled by an advanced LIGO detector ($r_0 = 355\,\mathrm{Mpc}$) in several matter dominated FRW cosmological models. The intrinsic chirp mass of all systems is assumed to be $1.19\,\mathrm{M}_\odot$. Six different models are shown, exploring two different h (0.5 and 0.8) and three different q_0 (1/4, 1/2 and 3/4). The closely spaced curves with co-located extrema are of the same h and differ only in q_0. Note the strong dependence of $P(\mathcal{M}|\rho_0, \mathcal{C}, \mathcal{D})$ on h and the weaker, but still significant, dependence on q_0: the dotted and solid curves correspond to flat cosmological models ($q_0 = 1/2$), the long-dash and dot-long-dash curves correspond to open cosmological models ($q_0 = 1/4$), and the short-dash and dot-short-dash curves correspond to the closed models ($q_0 = 3/4$). In general the smaller q_0, the more compressed the spectrum and the smaller the tail at large $\mathcal{M}$.

Since the abscissa $\mathcal{M}$ is related to redshift according to $\mathcal{M} = (1+z)\mathcal{M}_0$ figure 8 also shows the redshift of the preponderance of catalog events. For $h = 0.8$ most events are at a redshift of 9%, while for $h = 0.5$ most events are at a redshift of 14%.

More generally, neutron star masses are not all identical; correspondingly, $\mathcal{P}(\mathcal{M}_0)$ is not as simple as a δ-function. Modeling the neutron star mass distribution as uniform between lower bound m_l and upper bound m_h leads to the intrinsic chirp mass distribution $\mathcal{P}(\mathcal{M}_0)$ given by equation 2.11; the corresponding spectrum $P(\mathcal{M}|\rho_0, \mathcal{C}, \mathcal{D})$ can be determined through equations 4.26 and 4.27. Figure 9 shows the spectrum $P(\mathcal{M}|\rho_0, \mathcal{C}, \mathcal{D})$ for four

different matter-dominated Einstein-deSitter cosmological models corresponding to two different h (0.5 and 0.8) and two different neutron star mass distributions: one set of curves corresponds to the assumption that $\mathcal{M}_0 = 1.19\,\mathrm{M}_\odot$ for all binary systems, while in the second set the binary component masses are assumed to be uniformly distributed between $1.29\,\mathrm{M}_\odot$ and $1.45\,\mathrm{M}_o dot$. For all models shown $r_0 = 355\,\mathrm{Mpc}$ and $\rho_0 = 8$.

As m_l and m_h approach m_0, $\mathcal{P}(\mathcal{M}_0)$ approaches $\delta(\mathcal{M}_0 - m_0)$. The dependence of $P(\mathcal{M}|\rho_0, \mathcal{I})$ on q_0, shown in figure 8, is similar but not identical to its dependence on $m_h - m_l$ (for constant m_0): variations in q_0 shift the spectrum's large $\mathcal{M}$ tail, while increasing $m_h - m_l$ increases the spectrum's overall breadth.

V. CONCLUSIONS

Observations of binary inspiral in a single interferometric gravitational wave detector can be cataloged according to signal strength (as measured by signal-to-noise ratio ρ) and chirp mass $\mathcal{M}$. The distribution of events in a catalog composed of observations with ρ greater than a threshold ρ_0 depends on the Hubble expansion, deceleration parameter, and cosmological constant, as well as the distribution of component masses in binary systems and evolutionary effects (though for neutron star binary observations evolution is not expected to be important). In this paper I find general expressions for the distribution with ρ and $\mathcal{M}$ of cataloged events, valid in any homogeneous and isotropic cosmological model; I also evaluate those distributions explicitly for matter-dominated Friedmann-Robertson-Walker models and simple models of the neutron star mass distribution.

These distribution have two immediate, practical uses in gravitational-wave data analysis for interferometric detectors: first, when evaluated for with the cosmological parameters reflecting our current best understanding of the universe, they are the prior probabilities which, together with the matched-filtered detector output, form the likelihood function and determine the posterior probability that an inspiral has been detected; second, when compared with the observed distribution in ρ and $\mathcal{M}$ of many separate binary inspiral observations, they are used to infer new and more informed estimates for the cosmological parameters that describe the universe.

The signal-to-noise ratio ρ of a binary inspiral event is a detector-dependent measure of the signal strength from a radiation source that is estimated in the course of making an observation. The normalization of ρ depends on the detector's noise power spectral density $S_n(f)$. In interferometric gravitational wave detectors like LIGO and VIRGO the normalization involves a characteristic distance r_0 and a function of the detector bandwidth ζ, both of which are depend on $S_n(f)$.

The characteristic distance r_0 gives an overall sense of the depth to which the detector can "see" binary systems whose radiation traverses the detector bandwidth, which is determined by ζ. Advanced LIGO interferometers are expected to be most sensitive to binary inspiral radiation in the bandwidth 30–200 Hz: over 90% of the signal-to-noise ratio is contributed by signal power in this narrow band.

When searching the output of a detector for the signal from a source an accurate model of the detector response is needed. The model need not be accurate over the entire frequency domain, but only over that part of the domain where the signal power overlaps with the

detector bandwidth. The dependence of ρ on ζ suggests the definition of a *bandwidth function* $\mathcal{B}$ for binary inspiral observations that will be useful for determining over what range approximate templates describing the detector response need be accurate.

Cosmological tests based on catalogs of binary inspiral observations with ρ greater than a threshold ρ_0 depend on the distribution of cataloged events with ρ and $\mathcal{M}$. Tests can make use of all the information available in the catalog or properly constructed summaries of the cataloged events. The sensitivity of the test depends on how the expected catalog distributions change with changing cosmological models.

For advanced LIGO detectors, the most distant neutron star binary inspiral events with signal-to-noise ratio greater than 8 will arise from distances not exceeding approximately 2 Gpc, corresponding to a redshift of 0.48 (0.26) for $h = 0.8$ (0.5). The depth is only weakly dependent on the range of neutron star masses or the deceleration parameter. As the binary system mass increases so does the distance it can be seen, up to a limit: in a matter dominated Einstein-deSitter cosmological model with $h = 0.8$ (0.5) the limit is approximately $z = 2.7$ (1.7) for binaries consisting of approximately $10\,\mathrm{M}_\odot$ black holes.

The distribution of catalog events with ρ depends primarily on h and is only very weakly sensitive to either q_0 or the range of neutron star masses; however, the chirp mass spectrum (*i.e.,* the distribution of catalog events with $\mathcal{M}$) is very sensitive to h and reasonably sensitive to both q_0 and the neutron star mass range. This suggests that the spectrum is an especially powerful tool for cosmological measurements. The dependence of the spectrum on q_0 and the neutron star mass distribution is similar (though not identical), suggesting that it may be difficult to determine these separately from observations. I am currently investigating this point and will report on it at a later time.

ACKNOWLEDGMENTS

I am grateful for the support of both the Alfred P. Sloan Foundation and the National Science Foundation (PHY 9308728).

REFERENCES

[1] A. Abramovici *et al.*, Science **256**, 325 (1992).

[2] C. Bradaschia *et al.*, Nucl. Instrum. Methods Phys. Research **A289**, 518 (1990).

[3] K. S. Thorne, in *300 Years of Gravitation*, edited by S. Hawking and W. Israel (Cambridge University Press, Cambridge, 1987), pp. 330–458.

[4] L. S. Finn and D. F. Chernoff, Phys. Rev. D **47**, 2198 (1993).

[5] D. F. Chernoff and L. S. Finn, Astrophys. J. Lett. **411**, L5 (1993).

[6] B. F. Schutz, Nature (London) **323**, 310 (1986).

[7] D. Marković, Phys. Rev. D **48**, 4738 (1993).

[8] P. Jaranowski and A. Krolak, Astrophys. J. **394**, 586 (1992).

[9] C. Cutler and É. Flanagan, Phys. Rev. D **49**, 2658 (1994).

[10] S. Wipf and L. S. Finn, Observing binary inspiral with a three-interferometer gravitational wave detector, in preparation.

[11] R. Narayan, T. Piran, and A. Shemi, Astrophys. J. Lett. **379**, L17 (1991).

[12] E. S. Phinney, Astrophys. J. **380**, L17 (1991).

[13] J. H. Taylor and J. M. Weisberg, Astrophys. J. **345**, 434 (1989).

[14] A. Wolszczan, Nature (London) **350**, 688 (1991).

[15] T. A. Prince, S. B. Anderson, S. R. Kulkarni, and A. Wolszczan, Astrophys. J. Lett. **374**, L41 (1991).

[16] S. E. Woosley and T. A. Weaver, in *The Structure and Evolution of Neutron Stars*, edited by D. Pines, R. Tamagaki, and S. Tsuruta (Addison-Wesley, Redwood City, California, 1992), pp. 235–249.

[17] L. S. Finn, Phys. Rev. Lett. **73**, 1878 (1994).

[18] H. A. Bethe and G. E. Brown, Astrophys. J. Lett. **445**, L129 (1995).

[19] L. S. Finn, Phys. Rev. D **46**, 5236 (1992).

[20] L. S. Finn, in *Proceedings of the Cornelius Lanczos International Centenary Conference*, *SIAM Proceedings Series*, edited by J. D. Brown, M. T. Chu, D. C. Ellison, and R. J. Plemmons (SIAM, Philadelphia, 1994), pp. 479–481.

[21] T. A. Apostolatos, C. Cutler, G. J. Sussman, and K. S. Thorne, Phys. Rev. D **49**, 6274 (1994).

[22] C. Cutler *et al.*, Phys. Rev. Lett. **70**, 2984 (1993).

[23] L. E. Kidder, C. M. Will, and A. G. Wiseman, Phys. Rev. D **47**, 3281 (1993).

[24] C. S. Kochanek, Astrophys. J. **398**, 234 (1992).

[25] L. Bildsten and C. Cutler, Astrophys. J. **400**, 175 (1992).

[26] R. E. Vogt *et al.*, Proposal to the National Science Foundation, California Institute of Technology (unpublished).

[27] P. R. Saulson, Phys. Rev. D **42**, 2437 (1990).

[28] A. Gillespie and F. Raab, Phys. Lett. A **190**, 213 (1994).

[29] A. Gillespie and F. Raab, Thermally excited vibrations of the mirrors of laser interferometer gravitational-wave detectors, LIGO preprint 94-3, 1994, submitted to Physical Review D.

[30] S. Weinberg, *Gravitation and Cosmology: Principles and Applications of the General Theory of Relativity* (Wiley, New York, 1972).

[31] C. W. Misner, K. S. Thorne, and J. A. Wheeler, *Gravitation* (Freeman, San Francisco, 1973).

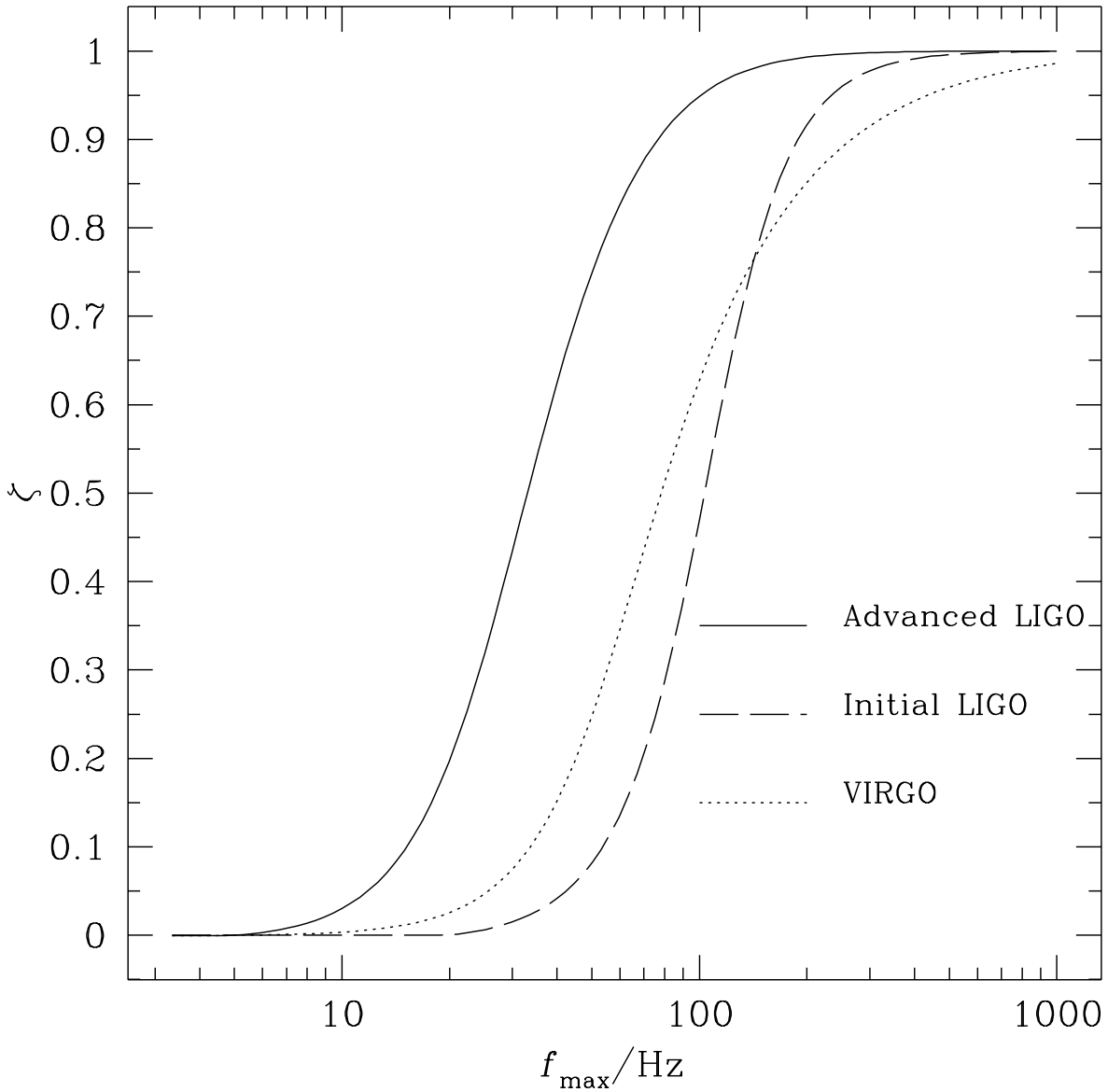

FIG. 1. The signal-to-noise ratio of the radiation from an inspiraling compact binary in an interferometric gravitational wave depends, through the function ζ (defined in eq. 3.6e) on the redshifted orbital frequency $f_{\rm max}$ of the system's last orbit before coalescence. Here is shown $\zeta(f_{\rm max})$ for initial LIGO (dashed), VIRGO (dotted) and advanced LIGO (solid) interferometers. For more detail, see the discussion in section III F and III D.

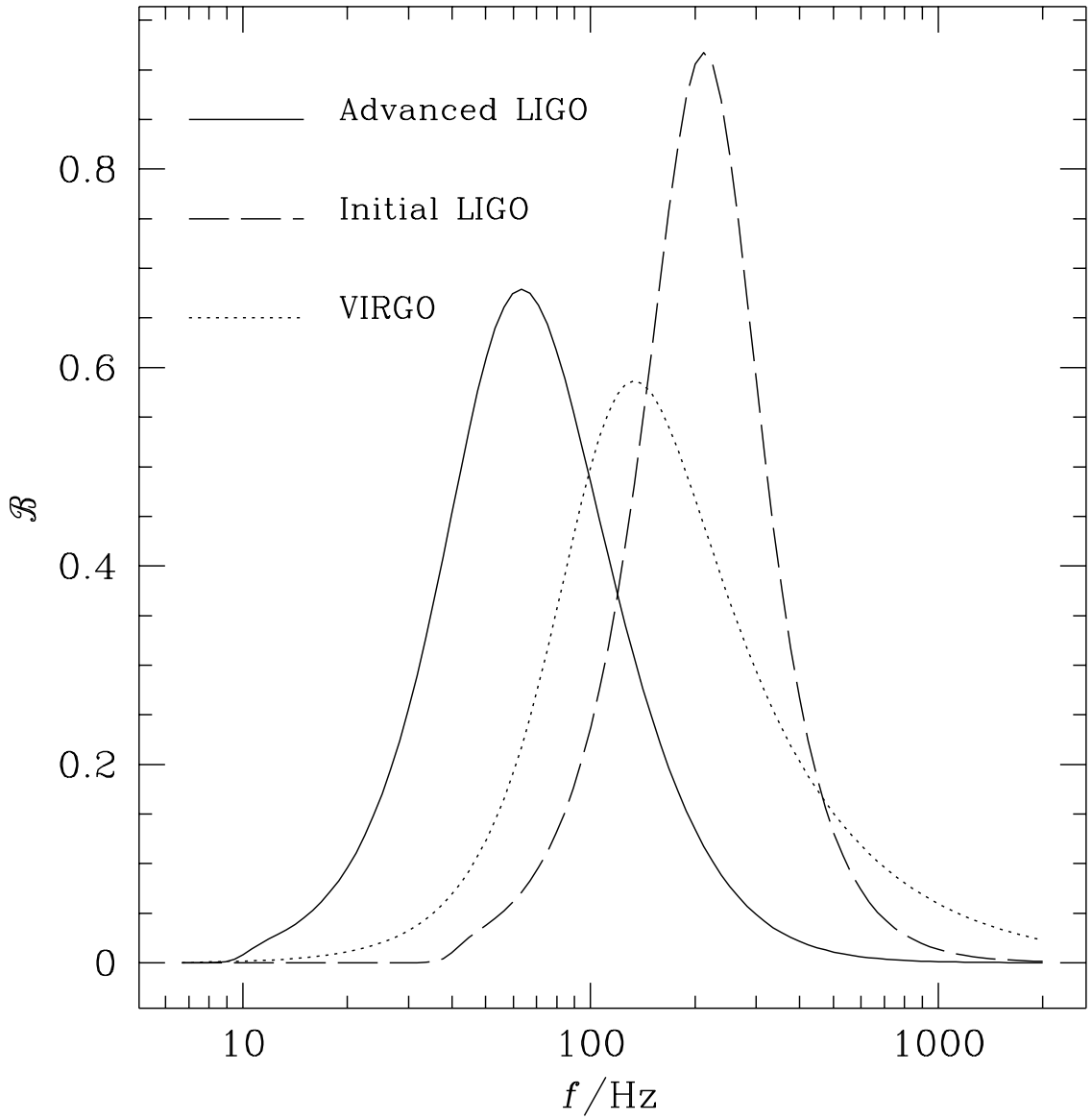

FIG. 2. The bandwidth function $\mathcal{B}(f)$ (defined in eq. 3.10) describes the fraction of ρ^2 contributed by signal power at frequency f in a logarithmic frequency interval. Here is shown $\mathcal{B}$ for initial LIGO, VIRGO and advanced LIGO interferometers. The bandwidth function is especially useful for determining over what frequency interval an approximate model of the detector response to the radiation, which might be used for identifying the presence of a signal in detector output, must accurately mimic the real detector response. For more details see the discussion in section III D 2.

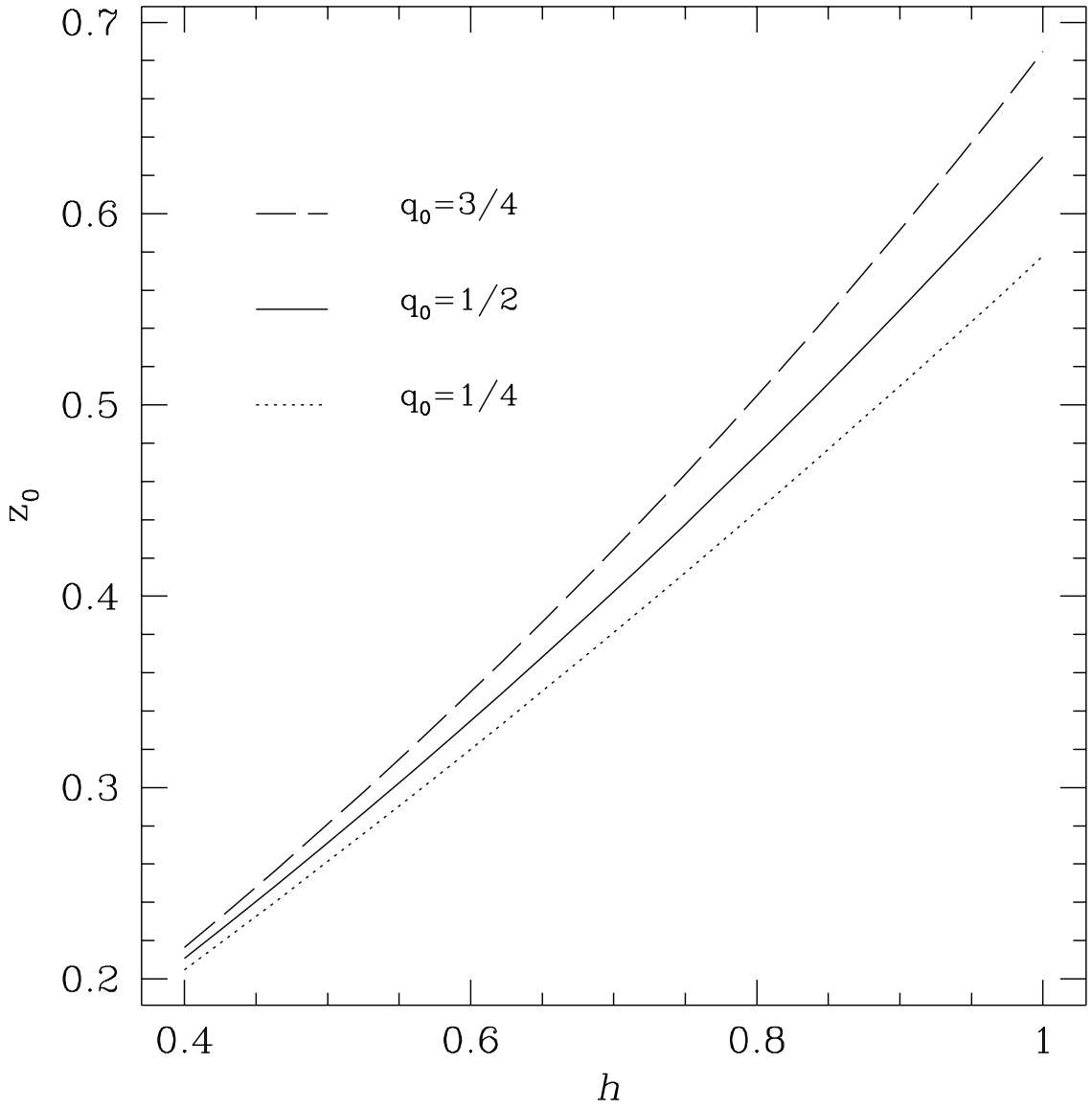

FIG. 3. The distance to the farthest inspiraling binary system with signal-to-noise ratio ρ greater than a threshold ρ_0 depends on the detector noise spectrum, the binary system component masses, and the cosmological model. Shown here is the redshift to the farthest ns-ns binary system observable with $\rho \geq 8$ in an advanced LIGO detector as a function of the Hubble parameter h (the Hubble constant in units of 100 Km/s/Mpc). The three curves represent matter dominated Friedmann-Robertson-Walker cosmological models with different q_0: a closed model with $q_0 = 3/4$ (dashed curve), a flat model ($q_0 = 1/2$, solid curve), and an open model with $q_0 = 1/4$ (dotted curve). For more discussion see IV D.

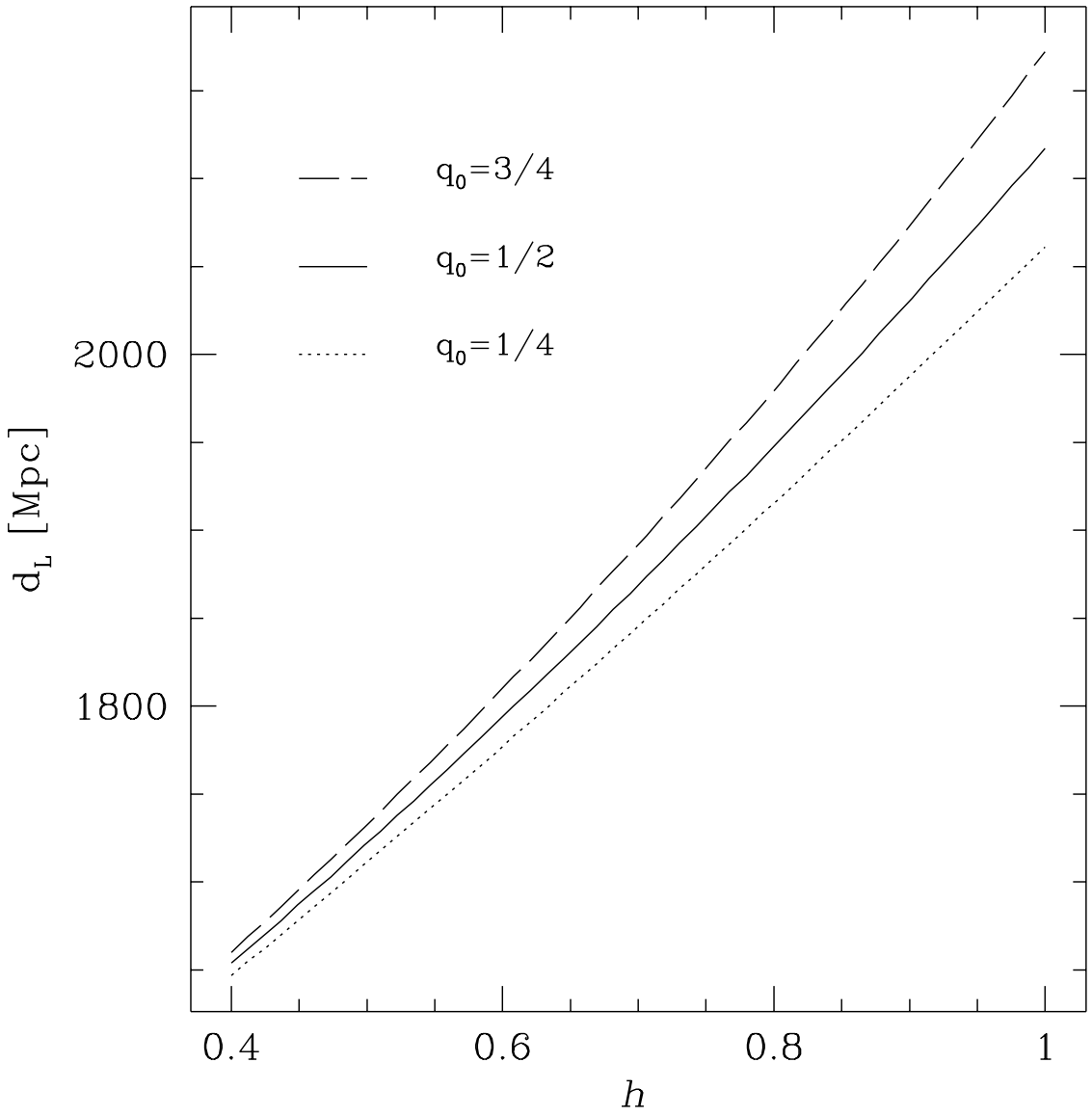

FIG. 4. The same as figure 3, except shown here is the luminosity distance instead of the redshift.

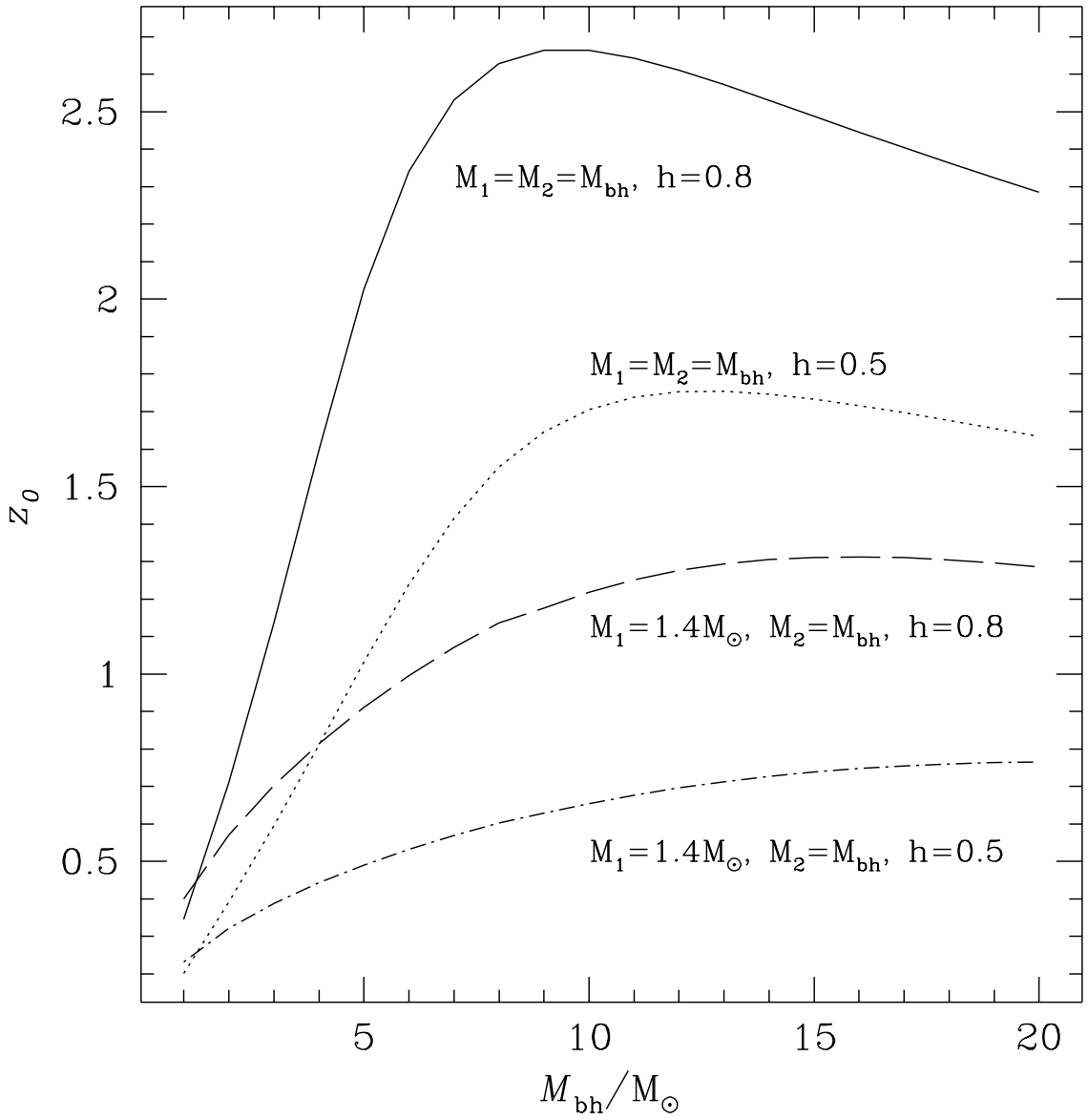

FIG. 5. The expected redshift to the farthest inspiraling binary system observed by an advanced LIGO detector with $\rho \geq 8$ in matter-dominated Einstein-deSitter cosmological models ($q_0 = 1/2$). Results for symmetric binary systems, consisting of two components each of mass $M_{\rm bh}$, and asymmetric binary systems, consisting of a $1.4\,{\rm M}_\odot$ component and a $M_{\rm bh}$ component, are shown for $h = 0.8$ and $h = 0.5$. The maximum observable depth at any signal-to-noise threshold is limited by the cosmological model and the properties of the detector; for advanced LIGO interferometers and $\rho_0 = 8$ it peaks for symmetric binaries composed of $10\,{\rm M}_\odot$ black holes. For more discussion see section IV D.

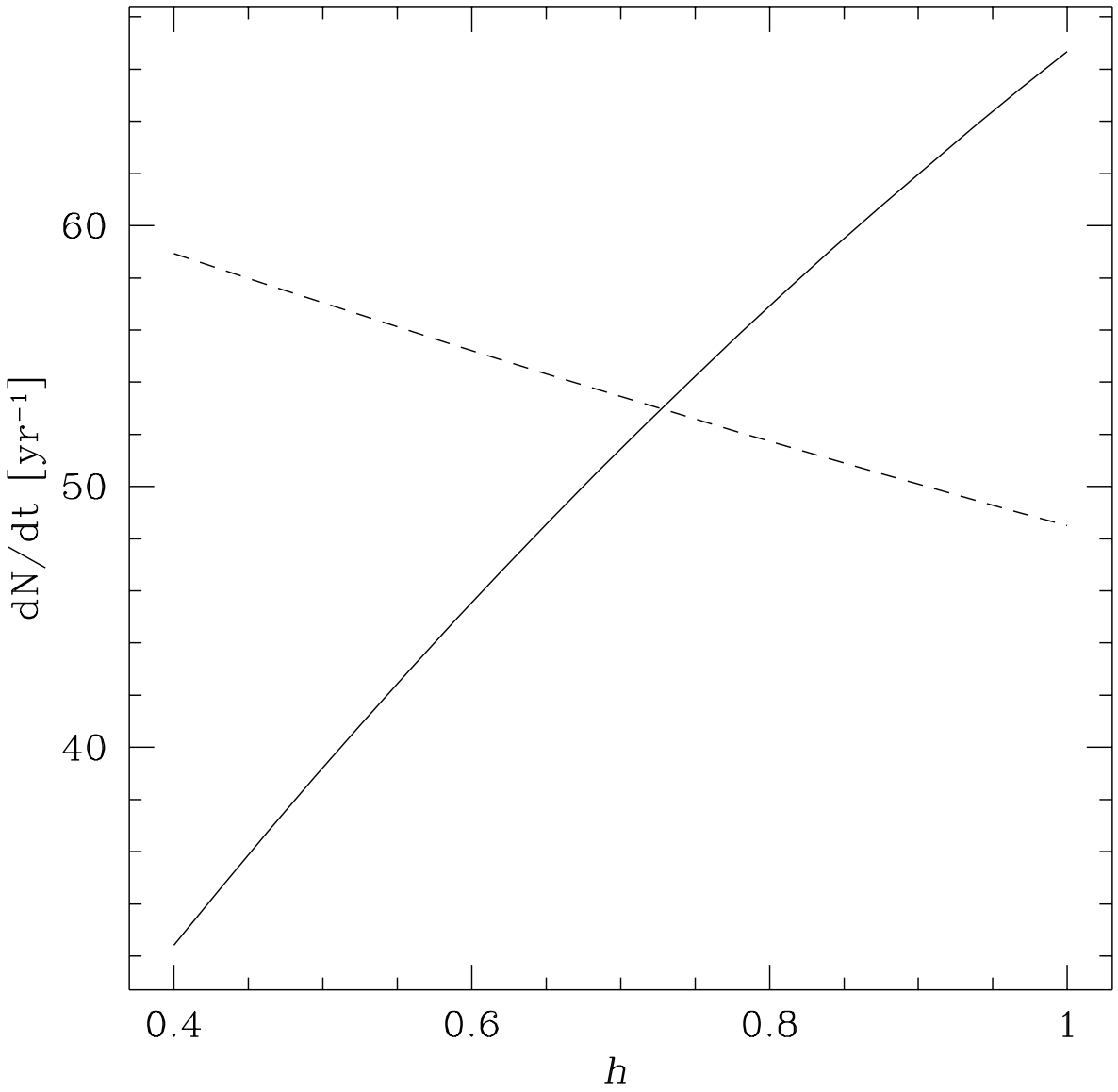

FIG. 6. The rate of ns-ns binary inspiral observations with signal-to-noise ratio greater than 8 in an advanced LIGO detector is largely insensitive to the neutron star mass range or the deceleration parameter in matter dominated Friedmann-Robertson-Walker cosmological models. The solid curve shows the expected rate in an Einstein-deSitter model as a function of the Hubble parameter h assuming the co-moving ns-ns binary coalescence rate density at the current epoch is $1.1h\,\mathrm{Mpc}^{-3}\,\mathrm{yr}^{-1}$ (solid curve); the dashed curve shows the same assuming the rate density is $8\times10^{-8}\,\mathrm{Mpc}^{-3}\,\mathrm{yr}^{-1}$, which is independent of h. For more discussion see section IV E.

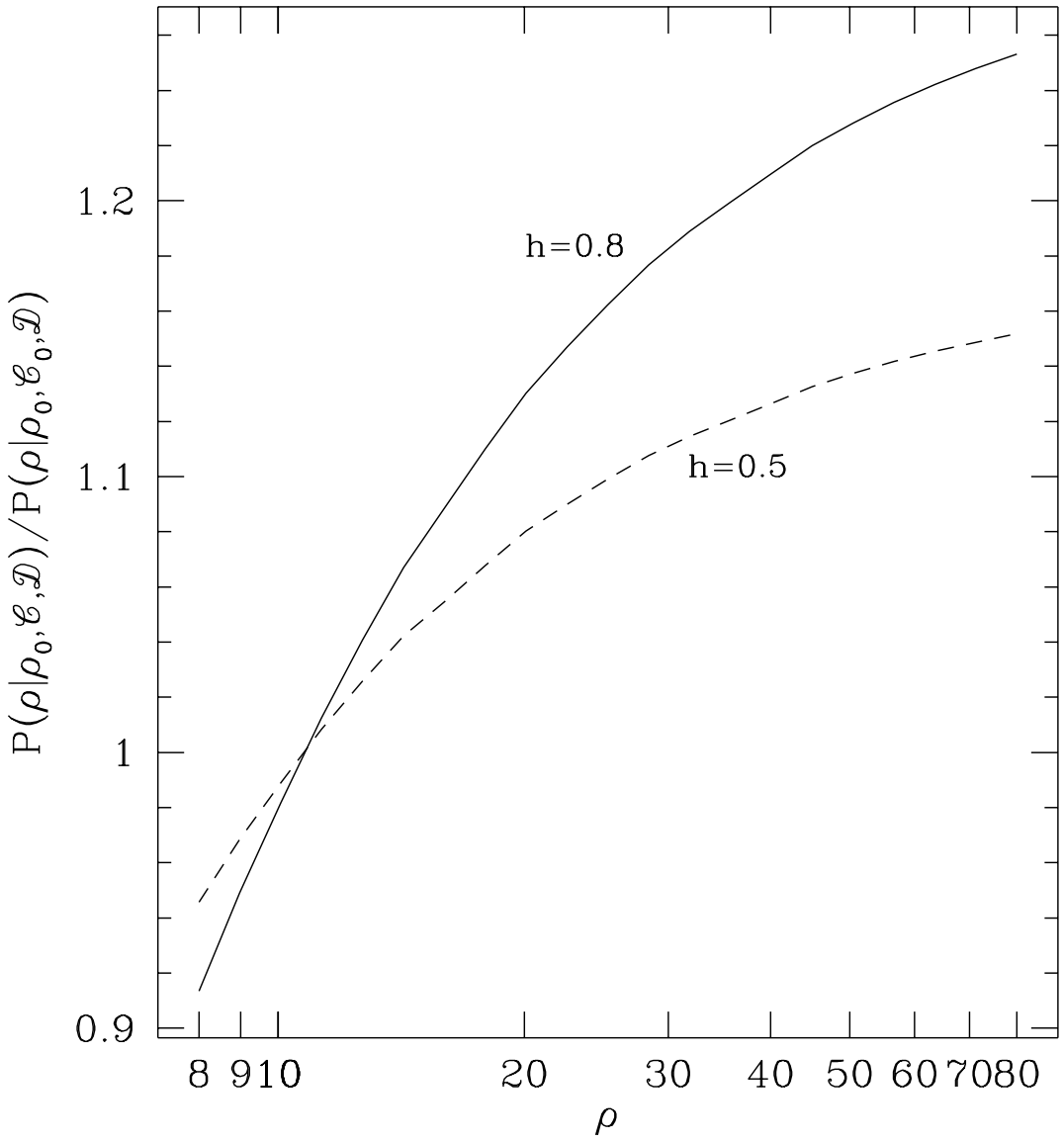

FIG. 7. The expected distribution of ns-ns inspiral events with ρ greater than 8 in advanced LIGO detectors depends almost exclusively on the Hubble parameter h. Shown here is the ratio of the distribution in two matter dominated Friedmann-Robertson-Walker cosmological models to the distribution expected in a flat and static cosmological model. For more details see section IV E 1.

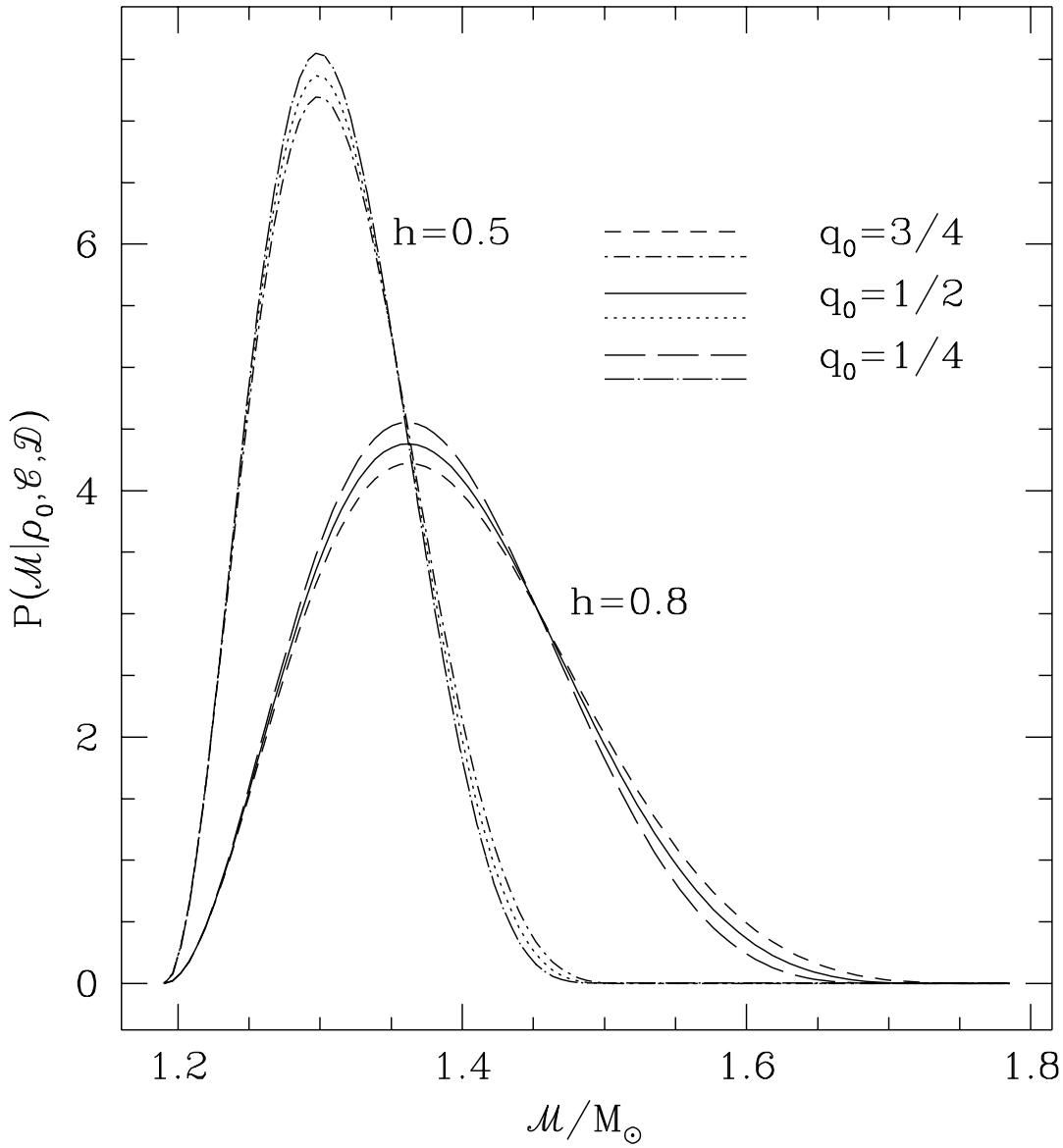

FIG. 8. A binary system's observed chirp mass $\mathcal{M}$ depends on its redshift; consequently, a ns-ns binary inspiral sample will show a range of chirp masses corresponding to the range of system redshifts. Shown here is the expected distribution of $\mathcal{M}$ for binary systems consisting of two $1.37\,M_\odot$ neutron stars with $\rho > 8$ in advanced LIGO detectors for open ($q_0 = 1/4$), flat ($q_0 = 1/2$) and closed ($q_0 = 3/4$) matter-dominated Friedmann-Robertson-Walker cosmological models with $h = 0.5$ and $h = 0.8$. In all cases, as q_0 increases the tail of the chirp mass spectrum is extended. For more details, see the discussion in IV F.

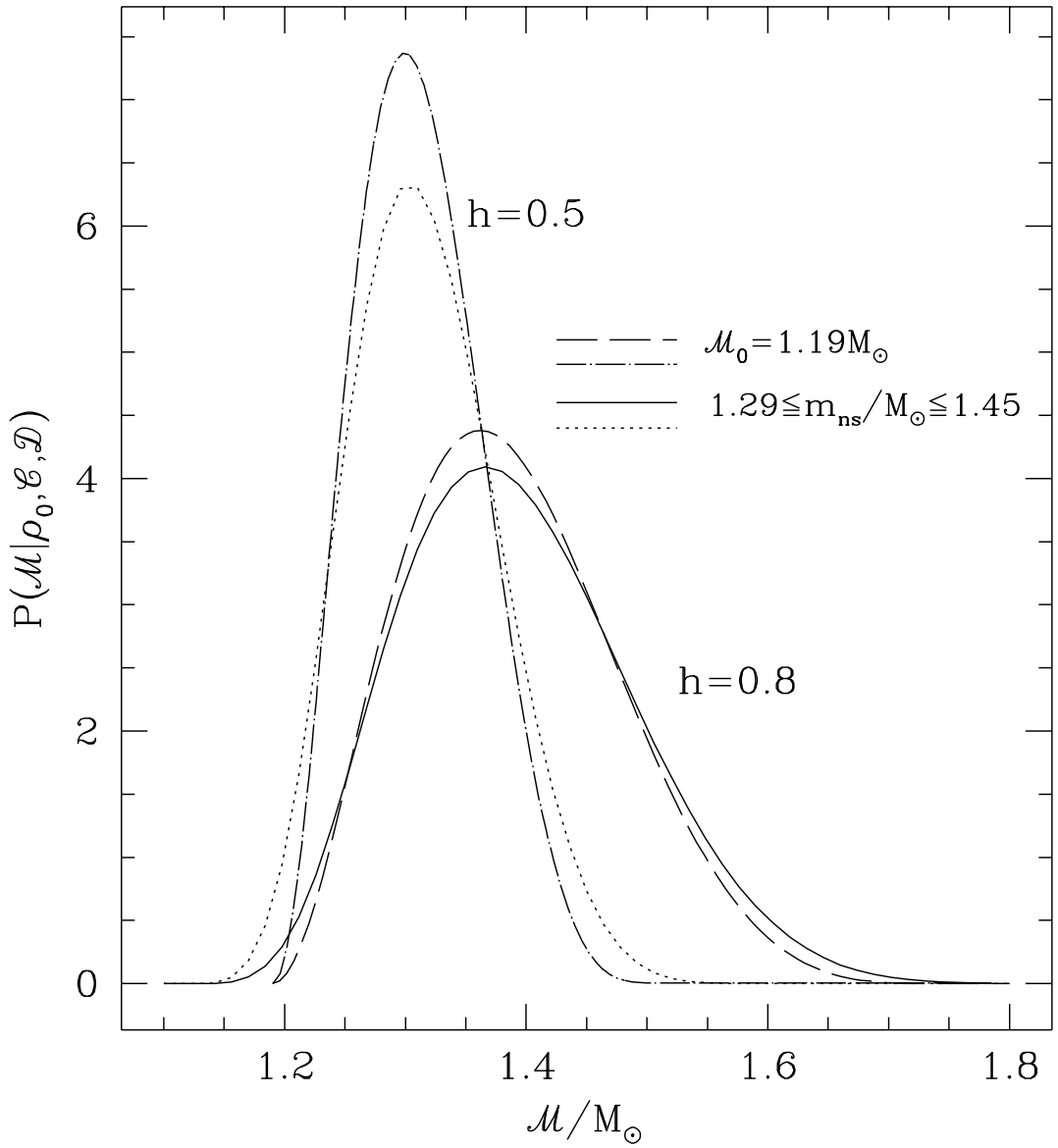

FIG. 9. Neutron stars do not all share the same mass, although indications are that the mass range is small. Shown here is the expected chirp mass distribution for observations with $\rho > 8$ made in an advanced LIGO detector for two different matter-dominated Einstein-deSitter cosmological models ($q_0 = 1/2$ and $h = 0.5$ or $h = 0.8$) and two different neutron star mass distributions. In the first distribution all binaries are assumed to have intrinsic chirp mass $\mathcal{M}_0 = 1.19\,\mathrm{M}_\odot$, while in the second the binary component masses are assumed to be uniformly distributed between lower bound $1.29\,\mathrm{M}_\odot$ and upper bound $1.45\,\mathrm{M}_\odot$. As the mass distribution broadens, the chirp mass spectrum also broadens. It does so nearly symmetrically; in contrast, variations in q_0 for fixed mass distribution (shown in figure 8) alter the large $\mathcal{M}$ tail of the spectrum, leaving the small $\mathcal{M}$ tail essentially unchanged. For more details see section IV F.